energy&fuels

pubs.acs.org/EF

Review

Fabrications and Applications of Micro/Nanofluidics in Oil and Gas Recovery: A Comprehensive Review

Junchen Liu, Yandong Zhang, Mingzhen Wei, Xiaoming He, and Baojun Bai*

Cite This: *Energy Fuels* 2022, 36, 9904−9931

Read Online

ACCESS | Metrics & More | Article Recommendations

ABSTRACT: Understanding fluid flow characteristics in porous medium, which determines the development of oil and gas oilfields, has been a significant research subject for decades. Although using core samples is still essential, micro/nanofluidics have been attracting increasing attention in oil recovery fields since it offers direct visualization and quantification of fluid flow at the pore level. This work provides the latest techniques and development history of micro/nanofluidics in oil and gas recovery by summarizing and discussing the fabrication methods, materials and corresponding applications. Compared with other reviews of micro/nanofluidics, this comprehensive review is in the perspective of solving specific issues in oil and gas industry, including fluid characterization, multiphase fluid flow, enhanced oil recovery mechanisms, and fluid flow in nano-scale porous media of unconventional reservoirs, by covering most of the representative visible studies using micro/nanomodels. Finally, we present the challenges of applying micro/nanomodels and future research directions based on the work.

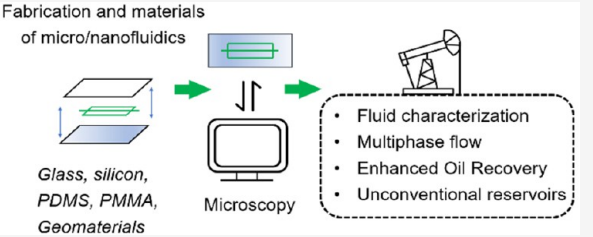

1. INTRODUCTION

Production of oil and gas, the most essential energy resources, has been studied by petroleum engineers for decades by using macroscopic and microscopic experimental methods. Oil recovery processes involve various complex fluid flows in porous media, such as water and oil flow,[1] gas and liquid flow,[2] solute and particle transport,[3] miscible and immiscible flow,[4] etc. Understanding of fluid flow from the reservoir-scale to the well-scale and core-sample-scale is of great importance for field potential determination, production prediction, and decision-making to further production treatment. However, it is impossible to perform direct visualization of deeply buried reservoir formations. Therefore, conventional coreflooding and microfluidic models are used to mimic and visualize the fluid flow in reservoirs.

Although the natural core provides a good representation of reservoir porous media, it is not transparent to visible light. Researchers can collect data, such as flow rate and pressure difference, from coreflooding experiments, but it is difficult to directly observe the fluid behaviors inside. Advanced imaging techniques, such as microcomputed tomography (μCT), nuclear magnetic resonance spectroscopy (NMR) and X-ray and focused ion beam scanning electron microscopy (FIB), have been applied to reveal pore structure, fluid distribution and porosity, etc.[5] However, these techniques are too expensive to be applied. What is more, the long scanning time and complex data processing also limit study of the dynamic process. Further, fluid flows in coreflooding experiments do not have good repeatability because the pore structure of every natural core is unique.

Therefore, micro/nanofluidic models (micro/nanomodel) have advantages over coreflooding experiments at pore-level observation due to the following reasons. First, micro/nanomodel experiments can easily identify pore-scale flow by integration with microscopy, providing observation of the fluid−fluid interaction and the fluid−solid interaction. Compared with obtaining natural cores in deep reservoirs, micromodel fabrication is more available because they are mostly optically transparent materials (glass and polymers). Second, running a micro/nanomodel experiment requires less fluid and time because the micro/nanomodels have a very tiny pore volume, so-called "lab/reservoir on a chip",[6] which is commercially popular.[7] Third, micro/nanomodels have a good repeatability using high resolution and better controlled fabrication methods, which enables variable controlled. Overall, with the development of fabrication and imaging techniques, micro/nanomodels will keep benefiting the oil and gas industry in the future.

In the last decade, there were some reviews of microfluidics regarding two-phase flow in underground water resources, oil and gas production and geosciences.[8−10] The researchers reviewed micro/nanofluidics application in enhanced oil

Received: June 11, 2022
Revised: August 7, 2022
Published: August 22, 2022

recovery (EOR).[6,7,11] The reviews focused on either micro/nanomodels in a two-phase flow or on the application in EOR only. Jahanbakhsh et al. collected microfluidics applications in two-phase flow and EOR.[12] However, none of them investigated and summarized the micro/nanofluidics application in view of solving specific issues in petroleum engineering, such as mechanisms of low-salinity water flooding, disproportioned permeability reduction of gel treatment and non-Darcy flow in unconventional reservoirs. To understand fluid flow characteristics in porous medium, a rapid increasing interest of micro/nanofluidics has been applied in these specific issues, and there is an urgent need to review and summarize fabrications and applications of micro/nanofluidics in oil and gas recovery.

In this work, we review the fabrication methods and common materials of micro/nanomodels. A summary of the fabrication methods and materials is presented in the review including the advantages and limits. Then we review the application of micromodels in oil and gas recovery regarding fluid characterization, multiphase fluid flow, EOR and unconventional reservoirs. Finally, we propose the challenges and outlook of micro/nanomodels in the oil and gas industry.

2. MICRO/NANOFLUIDIC MODELS FABRICATION METHODS

Micro/nanomodels span from the simplest designs in terms of 1D to complex structures of 2D and 3D. The fabrication procedure needs to be accurate and efficient. A simple micromodel can be fabricated by simply using glass tubes or capillaries, called a basic geometry model. Most micromodels are fabricated by nonadditive, additive and packing particle methods, which will be discussed in the following.

2.1. Nonadditive Manufacturing. Nonadditive manufacturing refers to forming micro/nanomodels by removing or shaping materials, including photolithography and shaping. The key to photolithography is transferring designed patterns from a mask to a photoresist layer on substrates. Shaping means giving a specific shape to the microfluidic materials by various methods, such as etching, soft lithography, laser engraving and hot embossing.[10]

2.1.1. Photolithography. Photolithography is one of the most widely used techniques to fabricate microfluidic models in which designed patterns of micromodels are formed by using UV light to shape a photoresist material on a substrate as shown in Figure 1. The

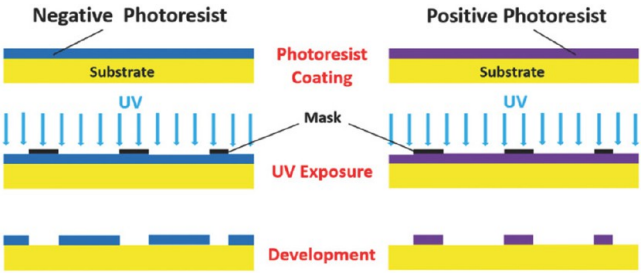

Figure 1. Procedure of photolithography using positive or negative photoresists. Reproduced with permission from ref 10. Copyright 2018 Small.

first step of the photolithography process is designing a photomask on software, such as CAD, then the photomask can be printed on films using laser printers.[13,14] The second step is placing the photomask onto a substrate of which the surface is already coated with a photoresist layer. Coating is achieved by spraying the photoresist onto a spinning wafer (substrate), which is usually glass or silicon, then the photoresist is heated (soft baking) for removing volatile solvents and preharden. Besides, the thickness of the coated layer is important because it is related to the geometry of the flowing channel. The thickness can be controlled by viscosity of the photoresist solution, the spinning speed and time.[15] The next step, known as "soft baking," involves placing the substrate on a heated plate or in an oven to evaporate the photoresist's volatile solvent. The third step is exposing the photoresist layer where it is not covered by a photomask to UV light, and the exposed material will become either insoluble or soluble to a photoresist developer solution depending on the type of photoresist. A positive photoresist is a type of photoresist in which the portion of the photoresist that is exposed to light becomes soluble to the photoresist developer, and it is usually a photodecomposing material. A negative photoresist is a type of photoresist in which the portion of the photoresist that is exposed to light becomes insoluble to the photoresist developer, and it is usually a photopolymeric/photo-cross-linking material. After a wash treatment with a developer solution, the "hard baking" process is necessary to harden the photoresist and enhance its adhesion to the substrate when the photolithography process is completed, and the combination of the substrate and the remaining photoresist can be bonded with glass plates to fabricate micromodels directly.[10] However, the combination is more often used as a photoresist master mold for the replica, so-called soft lithography.

2.1.2. Shaping. 2.1.2.1. Replica Molding. The replica molding process can be separated into two parts: fabrication of the master mold and use of the mold to generate the replica (Figure 2). After

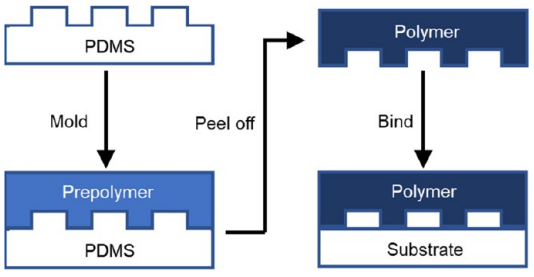

Figure 2. Schematic illustration of replica molding.

lithography development, the combination of the substrate and the photoresist can be utilized to create a master mold for thermally curable prepolymers, such as polydimethylsiloxane (PDMS), which makes it easy to generate small and fragile structures.[16] PDMS is a common polymer in the fabrication of micromodels because it is an elastomer and can be easily bonded with glass.[17,18] Before the polymerization, a negative template is filled with a prepolymer material, and polymer is formed and detached from the mold after polymerization. Then, the shaped polymer can be bonded with a glass plate, and a micromodel is fabricated. A large amount of micromodels can be fabricated with the same structures using the replica molding method, which is referred to as soft lithography.[10,12]

2.1.2.2. Etching. The etching method removes material of the substrate surface to create patterns and channels for micromodels, which can be divided into wet etching and dry etching. Wet etching is the process of removing materials with liquid chemicals (Figure 3). A glass substrate is commonly wet etched by buffered hydrofluoric acid (BHF) and a combination of hydrochloric acid (HCl) with hydrofluoric acid (HF), HNO_3, H_2SO_4 and H_3PO_4.[12] If the substrate is silicon, HNA and KOH can be used for the etching.[10] Besides, although a photoresist is usually stable against corrosive acid, a multilayer mask of metal, Cr/Au/Cr/Au, in combination with a thick photoresist can provide the best etching results in deep etching.[19,20] The etching can be controlled by acid type, glass type, acid concentration, temperature and reaction time.[20,21] It needs to be mentioned that wet etching is an isotropic reaction; the etching rate is equal in all directions, which means the acid can penetrate underneath of the protected mask, such as photoresist. This isotropic reaction cannot have perfect vertical walls of channels in substrates as shown in Figure 3 and Figure 4.[10,12,19] However, this imperfect trapezoidal shape can be used to generate a 2.5D micromodel by controlling the

https://doi.org/10.1021/acs.energyfuels.2c01943
Energy Fuels 2022, 36, 9904−9931

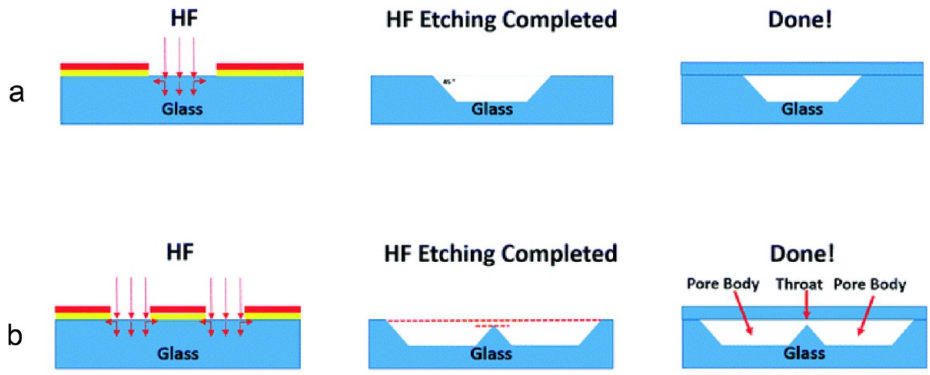

Figure 3. (a) Typical HF etching procedures to fabricate glass micromodels, trapezoidal cross section is formed due to the isotropic etching. (b) Fabrication of 2.5-D micromodel; throat is made by isotropic etching. Adapted with permission from ref 22. Copyright 2017 ROYAL SOCIETY OF CHEMISTRY.

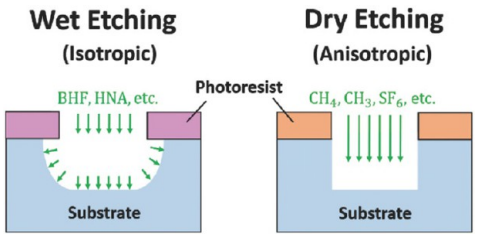

Figure 4. Schematic illustration of wet etching and dry etching. Adapted with permission from ref 10. Copyright 2018 Small.

etching depths of two neighboring pores, which enables a direction observation to capillary snap-off and a trapping phase due to the greater geometrical complexity in a 2D substrate plate.[22]

Dry etching includes usage of high energy of particle beams to destroy and remove material on a substrate,[23] such as metal, glass, semiconductor, polymer, oxide and photoresist.[24] For a typical glass etching, a chemically reactive plasma of gases, such as sulfur hexafluoride (SF_6), octafluorocyclobutane (C_4F_8), carbon tetrafluoride (CF_4) and fluoroform (CHF_3), is generated under low pressure by a strong radio frequency electromagnetic field, which is called plasma etching or reactive ion etching (RIE).[12,23] Dry etching on silicon or glass moves at a pace of less than 1 μm per minute, which is far slower than the pace for wet etching, which may move at up to 10 μm per minute,[10] resulting a better control of depth by simply stopping the plasma.[12] Although the dry etching method enables better control on the etching rate and direction (anisotropy), which results in a straight wall (Figure 4), it costs more than wet etching since it needs advanced facilities.

2.1.2.3. Laser Engraving/Ablation. Laser engraving has been used to prepare micromodels by directly removing materials on substrates (Figure 5) for many years.[25] Laser engraving does not require dangerous etchants, such as hydrofluoric acid, or heating of materials,[26,27] and it can be widely applied to many materials such as metals, polymers, ceramics, composites, semiconductors, diamond, graphite and glass.[28] The laser gases can be F_2, ArF, KrF, XeCl, XeF and CO_2, causing different laser wavelengths.[28,29] Laser ablation involves absorption of the laser radiation by the material, which results in conversion of optimal energy to heat within a relatively small volume. Doryani et al. visualized asphaltene precipitation utilizing a micromodel fabricated by CO_2 laser engraving.[30] However, the typical resolution of laser engraving is in size of micrometers due to its diffraction limitation, which is not able to provide high accuracy of channels. Recently, it has been reported that New-Ge laser direct writing can improve the resolution to the nano-scale,[25] but it has not been applied in the oil and gas research yet.

2.1.2.4. Hot Embossing. The hot embossing technique shapes microstructures by stamping the specific patterns on a thermoplastic polymer substrate that is already heated or molten thermally, such as poly(methyl methacrylate) (PMMA), under a high pressure and high temperature. Stamping patterns need a mold that can be divided into two types: a single-stage mold and a roller-to-roller mold.[33] For conventional/single-stage hot embossing, two plates are combined to an applied load and generate microstructures as shown in Figure 6.[34] For roller-to-roller hot embossing, a polymer sheet is fixed and stamped by two rollers, among which one contains a micropattern and the other one is the supporting roller. The polymer sheet is continuously passed through the rollers as shown in Figure 6.[35] Hot embossing is a small-scale, low-cost processing technology that can deliver products to the market in a short time.[36] The major challenge

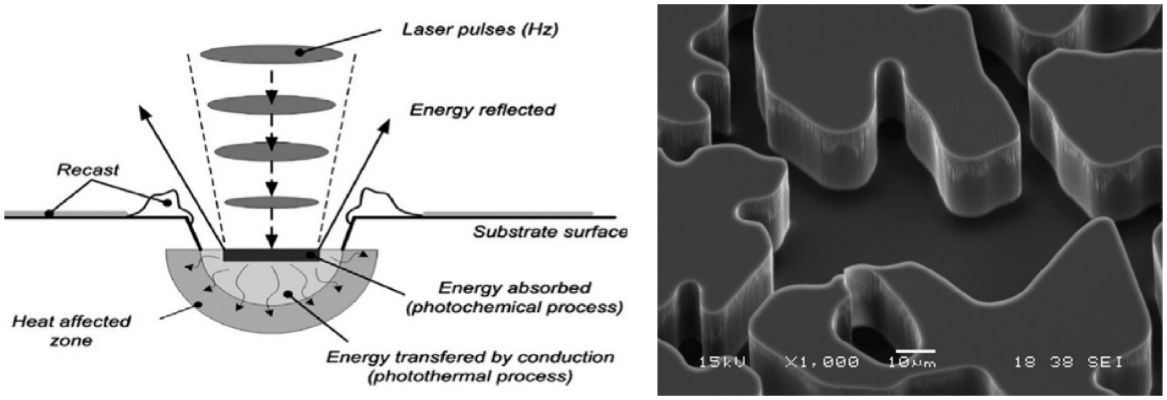

Figure 5. Laser engraving (left). Reproduced with permission from ref 31. Copyright 2007 Elsevier. Glass micromodel by laser engraving (right). Reproduced with permission from ref 32. Copyright 2015 Elsevier.

https://doi.org/10.1021/acs.energyfuels.2c01943
Energy Fuels 2022, 36, 9904−9931

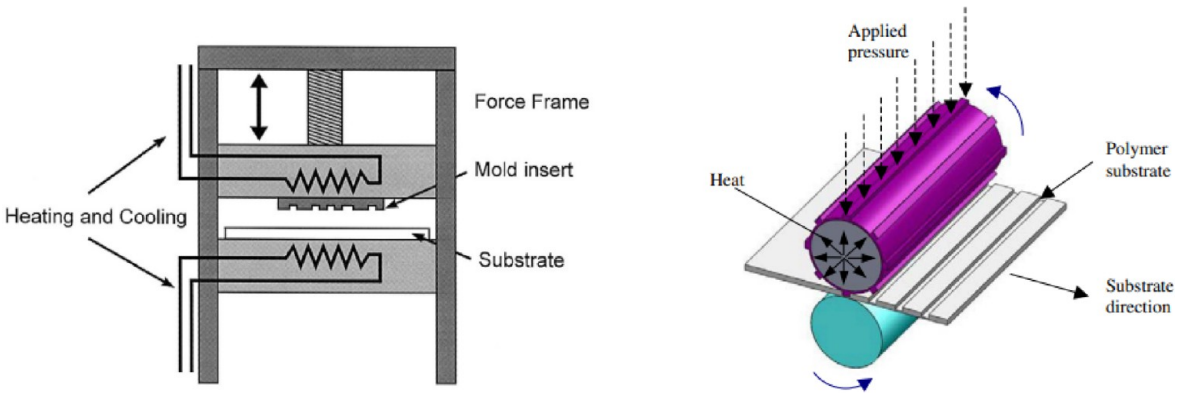

Figure 6. Schematic of conventional hot embossing (left). Reproduced with permission from ref 34. Copyright 2000 Elsevier. Hot roller embossing (right). Reproduced with permission from ref 35. Copyright 2009 IOP Publishing.

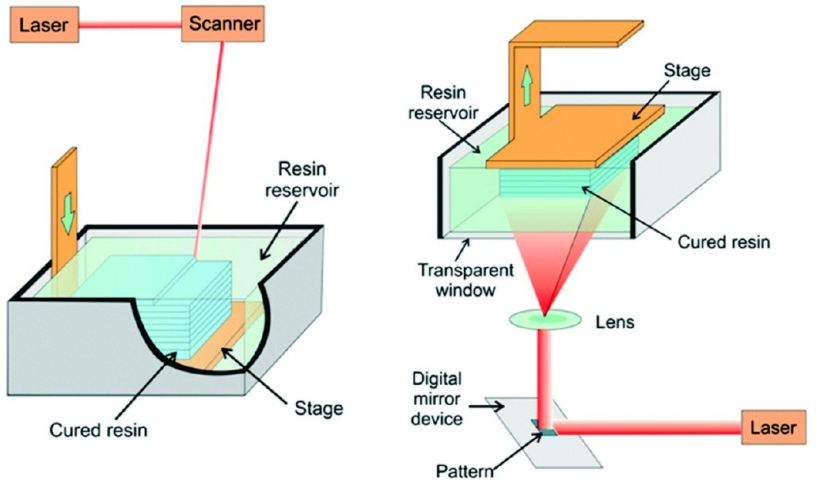

Figure 7. Schematic of stereolithography (lift) and digital light procession (right). Reproduced with permission from ref 38. Copyright 2016 ROYAL SOCIETY OF CHEMISTRY.

is to ensure complete filling of the cavity on the embossing tool with the work material to achieve the maximum accuracy.[33]

2.2. Additive Manufacturing. In the creation of complicated microfluidic models, nonadditive manufacturing is constrained due to the nature of fabrication devices and methods. 3D printing, one of additive manufacturing methods, has attracted attention to fabricate microfluidic systems because of its fast prototyping, complexity in model geometry, effective cost and waste reduction.[37,38] For a typical manufacturing process, successive layers of materials are laid down on top of each other until a 3D object is formed.[12] The 3D printing method includes a photocuring method, extrusion-based 3D printing and a photomelting method,[39] of which stereolithography is the most common method for microfluidic models.[38] As a fast-growing method, stereolithography will bring a lot of applications in micromodel fabrication in the future, such as its combination with soft lithography as a mold production method. In addition to 3D printing, thin film deposition, as a fast and low-cost method, is also an additive manufacturing method to produce micro/nanochannels.

2.2.1. Photocuring Method. The photocuring method can be divided into stereolithography (SLA) and digital light procession (DLP) as shown in Figure 7.[39] SLA is the most popular 3D printing approach to directly print and create visible microfluidic devices, in which a 3D object is constructed layer-by-layer using controlled solidification of a liquid resin by photopolymerization.[9] For every deposited layer, a laser beam will selectively project a designed pattern on the layer to conduct polymerization. After the deposition and polymerization are completed, the unpolymerized are washed and UV light is often used to improve mechanical properties of the model.[8,10] Digital light procession, as another more recent photocuring method, also uses laser/UV lamp and photosensitive resin to form patterns of each layer. The difference between DLP and SLA is that DLP uses a digital mirror device as a dynamic mask and the photosensitive resin is exposed to the laser/UV light through a mask, while SLA uses a moving laser directly.[39] The common materials of SLA and DLP are PDMS, poly(ethylene glycol) diacrylate and a clear resin.[37,40]

2.2.2. Extrusion-Based 3D Printing. Extrusion-based 3D printing is a widely used additive manufacturing technology to constitute a 3D object, among which fused deposition modeling (FDM) is the most typical one (Figure 8). FDM uses material that can be melted by heating to extrude the filament layer by layer. Each layer is piled on the past layer, and the past layer plays the role of positioning and supporting. The material hardens by spontaneous cooling immedi-

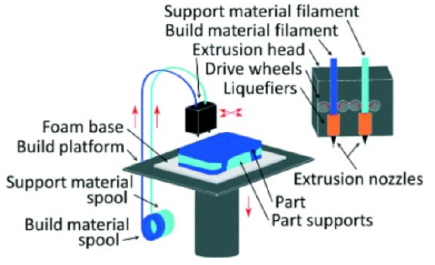

Figure 8. Schematic of fused deposition modeling. Reproduced with permission from ref 38. Copyright 2016 ROYAL SOCIETY OF CHEMISTRY.

https://doi.org/10.1021/acs.energyfuels.2c01943
Energy Fuels 2022, 36, 9904−9931

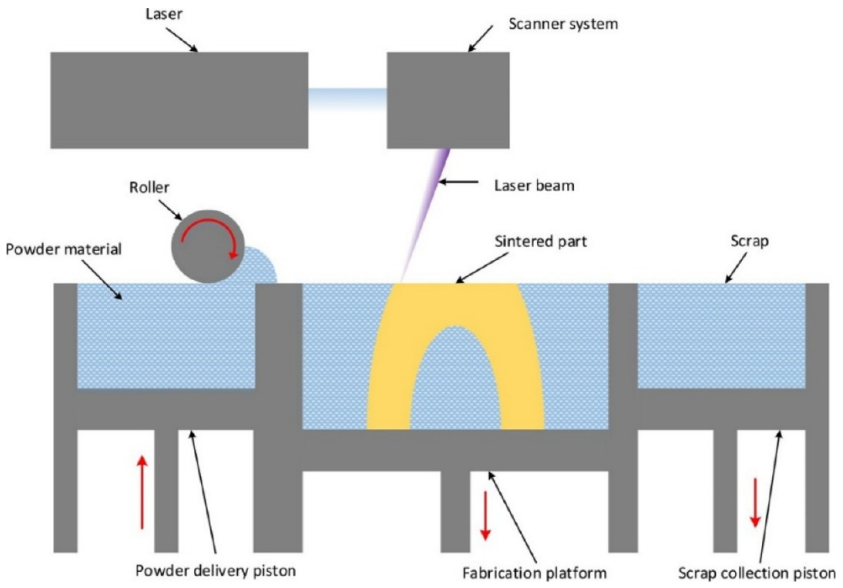

Figure 9. Schematic of selective laser sintering. Reproduced with permission from ref 39. Copyright 2016 John Wiley and Sons.

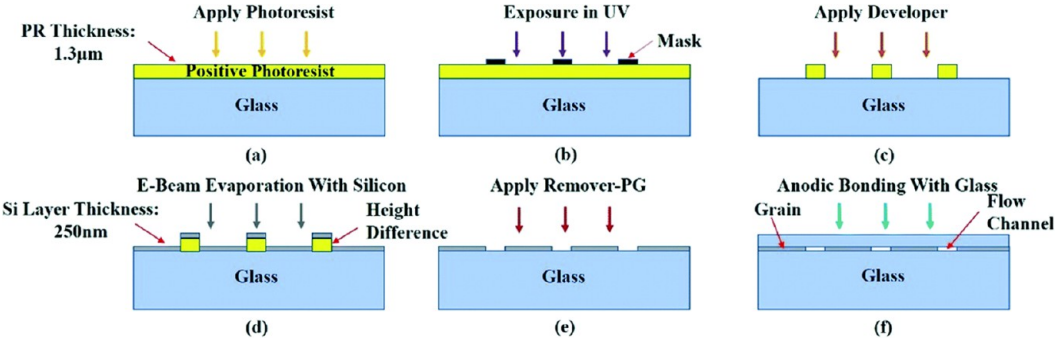

Figure 10. Combination of thin film deposition and lithography. Adapted with permission from ref 49. Copyright 2019 ROYAL SOCIETY OF CHEMISTRY.

ately after extrusion.[38,39] FDM has been used to print a wide range of cheap polymers like acrylonitrile butadiene styrene (ABS), polyethylene terephthalate (PET), polyamide and polystyrene. Although researchers try to improve the optical transparency of FDM-generated devices,[41,42] using FDM to make microfluidics is still limited by insufficient resolution, lack of structural integrity and low optical transparency of materials.[37,38,43]

2.2.3. Photomelting Technique. Compared with the photocuring technique, photomelting uses powdery materials rather than liquid materials, in which selective laser sintering (SLS), or called selective laser melting, is the main method (Figure 9). SLS is a rapid prototyping process that allows one to generate complex 3D objects by solidifying successive layers of a powder material, such as polymer, metal and ceramic, on top of each other, based on sintering (fusing) selected areas of the successive powder layers using thermal energy supplied through a laser beam.[44] The advantage of this technique over other 3D printing techniques is that various powders can produce materials that, when sintered, have a high purity, good strength and properties similar to those obtained by conventional fabrication processes.[45] The current micro SLS method has a resolution of 15 μm, but the technique is limited by controlling the resolution, removal of the unsintered powder, surface roughness and part removal.[46]

2.2.4. Thin Film Deposition. On top of 3D printing, thin film deposition also belongs to the additive manufacturing method, which can precisely control thin film thickness on a substrate with a high aspect ratio structure[47] (high aspect ratio can have a better observation and influence flow pattern). Generally, film material is released as atoms, molecules, or ions, and the released particles are deposited on the substrate to create a thin film.[48] For an energy field microfluidic system, only Zhang et al. combined this method with lithography to create silicon-based micromodels for an unconventional reservoir since it can precisely control film thickness and have a high aspect ratio structure (Figure 10).[49] The main disadvantage of thin film deposition is that the bonding strength is not high enough when the deposition film is very thin. While the other researchers usually apply thin film deposition as a protection layer[19] and mask[50] for wet etching or dry etching.

2.3. Packing Particles. Micromodels can be constructed by packing particles (glass beads, silica particle and geomaterial grains) in a glass container (box or tube), forming a 2D model or 3D model (Figure 11). The most common packing particles are glass beads in the size of micrometers, of which packing is normally achieved by vibrating the glass container while inserting the beads.[12] Then, depending on glass-beads size, the packing model is sintered at 850−900 °C for 1−10 min for solidification.[10] A regular or an irregular pore structure is formed by using the same or different sizes of beads. The fabrication of a glass-beads model is not complicated and expensive. Using confocal microscopy, a thin glass-beads model can reveal fluid flow in 3D structure, which is the most important advantage. However, the lower half of the model is still difficult to be observed,[8,12] and the shape of pore bodies in the structure is quite limited because it depends only on the diameter of beads and their arrangement. In addition, glass-bead packed models just represent a porous system rather than an actual reservoir rock.[7] To integrate more realistic surface mineralogy for rocks and soils in the packed beds, packing crushed rock or rock-forming mineral particles has been used

https://doi.org/10.1021/acs.energyfuels.2c01943
Energy Fuels 2022, 36, 9904−9931

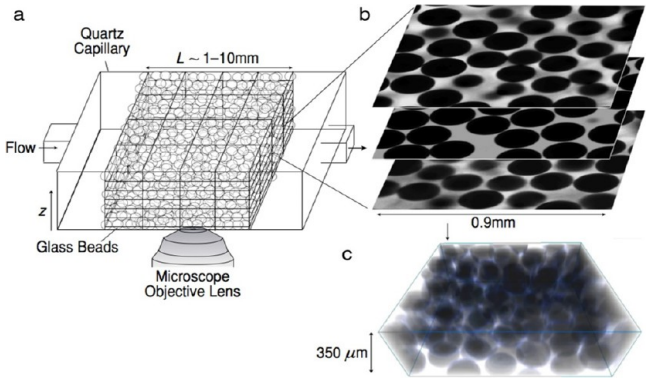

Figure 11. Illustration of 3D glass packed model and imaging of confocal microscopy. Reproduced with permission from ref 52. Copyright 2013 John Wiley and Sons.

to fabricate micromodels.[51] Overall, both the glass-bead packed model and the rock-particle packed model suffer from in-depth visualization.

The methods of manufacturing micro/nanofluidic models are summarized in Table 1.

3. MICRO/NANOFLUIDIC MATERIALS

Fabrication materials should be optically semi- or fully transparent to allow direct visualization of the fluid flow within micro/nanomodels. Also important are cost effectiveness and chemical stability of fabrication materials. Glass, silicon and polymers, such as PDMS and PMMA, are widely applied in the micromodel fabrications in the oil and gas industry meeting the requirements.[6,7,10,12] Here we will discuss the basic properties of these materials and their roles in fabricating different micro/nanomodels.

3.1. Glass. Glass has long been a preferred material because of its high transparency, low cost, hardness, chemical resistance and thermal stability (Figure 12). It is reported that glass has a high elastic modulus ranging from 50 to 90 GPa,[10] which enables it to tolerate high pressure, such as a few tens of MPa in fluid flow experiments.[53,54]

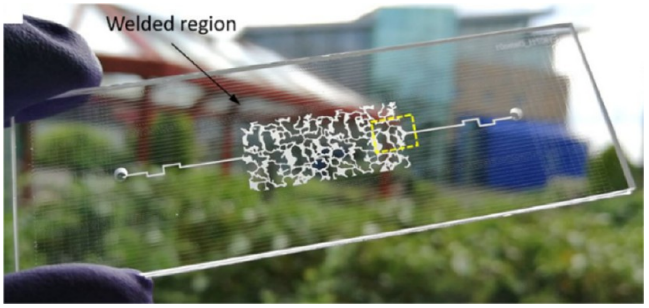

Figure 12. Glass model by laser engraving. Reproduced with permission from ref 27. Copyright 2019 Springer Nature.

Further, it is easy to change surface wettability of glass by different methods, such as hydrophilization with octadecyl trichlorosilane[11] and coating with calcium carbonate.[55] Another advantage of glass is that glass keeps its original properties after the bonding process. The most common glass used is borosilicate glass, which has low residual stress after bonding.[56] Bonding of glass material includes anodic bonding,[27] fusion bonding,[57] calcium-assisted bonding,[58] low-temperature bonding[59] and the adhesive bonding.[60] Besides, glass has good thermal stability that is enough to simulate reservoir conditions. Generally, glass can be used as substrates in photolithography and shaping methods, or glass matrix in particle packing methods. With the development of 3D printing techniques, the selective laser etching (SLE) technology has been proven to enable the fabrication of 3D microfluidic devices in glass.[61] Although glass is cheap, the fabrication of microfluidics can be very expensive and time-consuming, such as dry etching.[37] Besides, wet etching of glass is hard to be controlled and hazardous chemicals, such as HF, are produced. What is more, glass material is different from geomaterials, resulting in different wettabilities, surface roughnesses and pore geometries.

3.2. Silicon. Silicon has been the primary material in microfabrication for decades with well-established processes and fabrication methods (Figure 13). Extensively characterized surface modification properties based on the silanol group (−Si−OH), along with chemical

Table 1. Summary of Manufacturing Methods

	Manufacturing methods		Materials	Dimensions and resolutions	Features
Nonadditive	Photolithography		Glass, silicon and photoresist	2D, 1 μm	Well-established fabrication process, simple bonding, but unstable structure
	Shaping	Replica molding	Polymer, glass, silicon and photoresist	2D, 1 μm	Fast, cheap and mass production, but unstable structures
		Wet etching	Etchant, glass, silicon and photoresist	2D and 2.5D, 20 μm	Easy and cheap, but isotropic process
		Dry etching	Gases, glass, silicon and photoresist	2D and 2.5D, 10 nm	High accuracy, but limited depth and very expensive
		Laser engraving	Metal, polymer, glass	2D and 2.5D, 20 μm	No dangerous chemicals and various materials, but limited resolution
		Hot embossing	Thermoplastic polymer	2D and 3D, 100 nm	Low cost, repeatable and high accuracy, but challenge of cavity
Additive	Photocuring method	Stereolithography	Liquid photosensitive resin	2D and 3D, 100 μm	Low cost and good optical clarity, but limited material and resolution
		Digital light procession			
	Extrusion-based 3D printing	Fused deposition modeling	Polymer, metal	2D and 3D, 200 μm	Low cost and easily accessible, but low resolution and transparency
	Photomelting method	Selective laser sintering	Polymer, metal and ceramic	2D and 3D, 15 μm	Various materials and good strength, but expensive
	Thin film deposition		Silicon	2D, 250 nm	High aspect ratio structure, limited by bonding strength
Packing particles	Glass beads packed model		Glass	2D and 3D, 1 μm	Easy and cheap, but limited pore structure and challenge of replica
	Rock particle packed model		Geomaterials and glass	2D, 1 μm	Easy and cheap, but limited pore structure and challenge of replica

https://doi.org/10.1021/acs.energyfuels.2c01943
Energy Fuels 2022, 36, 9904−9931

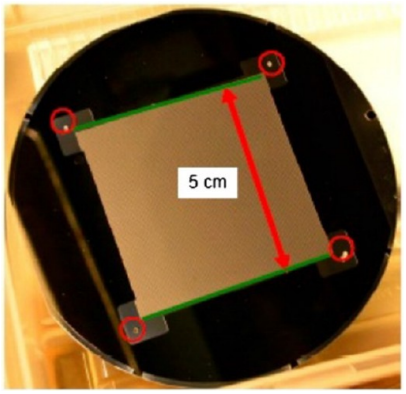

Figure 13. Silicon-based micromodel by etching. Reproduced with permission from ref 63. Copyright 2016 Elsevier.

resistance and flexibility in design, makes silicon a desirable material for the fabrication of microfluidic devices.[37] Moreover, silicon-based micromodels are better than glass-based micromodels for better quality control and high geometry resolution while still keeping the merits of glass, such as good chemical stability and feasible wettability alteration.[62] Further, silicon can withstand temperatures as high as 1400 °C and high elastic modulus (130−180 GPa).[10] Since silicon is translucent, direct visualization of fluid flow inside silicon structures is possible only when the surface of a silicon wafer is bonded to a transparent (typically glass) substrate.[12] Similarly with glass, silicon wafer can be used as a substrate in lithography, etching and hot embossing methods. Anodic bonding is the most common method for bonding silicon with glass, and silicon to silicon bonding can be achieved by fusion bonding.[56] However, the high elastic modulus and chemical stability of silicon complicate the model fabrication and make the fabrication very expensive.

3.3. PDMS. PDMS (polydimethyl siloxane) is an excellent material and will reign in the field of microfluidics for years due to the following reasons (Figure 14). First, it is an elastomer that is ideal for soft lithography and hot embossing with a thermal treatment temperature from 40 to 70 °C,[57] and its elastic modulus ranges from 1.32 to 2.97 MPa by tuning the cross-linking density.[64] Second, it is optically transparent, which enables a number of detection schemes (UV/vis absorbance and fluorescence).[18] Third, it is hydrophobic but can become hydrophilic by modification, such as plasma oxidation.[9] Fourth, PDMS is easily bonded with other materials and the bonding can be reversible or irreversible due to modification.[12] Finally, preparing PDMS templates is easier and less expensive as compared to the preparation of silicon or glass templates, and it is easy to peel PDMS off the templates after being cured due to its low surface energy.[57] Usually, PDMS is widely applied in soft lithography, photolithography, 3D printing and microfluidic switches.[40] While PDMS is very cheap and easy to treat, it reacts and absorbs fluids and chemicals that are commonly used in two-phase flow experiments, which results in swelling and deformation of network of micromodels.[8] In addition, wettability of treated PDMS (hydrophobic) is not stable because it degrades with time and recovers its hydrophobicity.[8] It needs to be mentioned that PDMS is gas-permeable, which limits the application in gas flow experiments.

3.4. PMMA. PMMA (poly(methyl methacrylate)) is a common thermoplastic, low cost and transparent polymer that has been widely used as a substrate material for microfluidic chips (Figure 15).

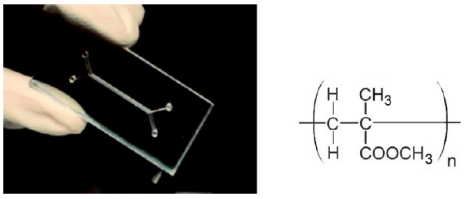

Figure 15. PMMA micromodel and molecular structure of PMMA. Adapted with permission from ref 67. Copyright 2019 ROYAL SOCIETY OF CHEMISTRY.

Compared with other materials, PMMA has its mechanical, thermal and chemical resistances between glass and PDMS,[9] with a glass transition temperature of 106 °C and an elastic modulus of 3.1 GPa. By heating or cooling the polymer at its glass transition temperature, the mobility of PMMA polymer chains can be controlled and the material can be in the liquid or solid phase.[35] Pore network structures on PMMA can be generated by either direct laser writing or 3D printing methods. Besides, the wettability of PMMA is easily treated with plasma treatment, UV/ozone exposure or chemical treatment.[51] The bonding techniques of PMMA includes thermal fusion, solvent bonding, ultrasonic welding and low temperature bonding.[57] PMMA usually provides a lower cost and easier manufacturing in micromodel fabrication than PMDS.[66] Although PMMA is resistant and stable to most inorganic chemicals, such as alkalis solution and acids, at room temperature, it is soluble in many common organic solvents, like ethanol and acetone.[9,10] Besides, it is difficult to have a high resolution of the structural features when PMMA is used in regular additive manufacturing.[57]

The materials for fabricating micro/nanofluidic models are summarized in Table 2. A fundamental weakness of the materials is that they have a very homogeneous composition, which means complex wettability, adsorption and other physicochemical properties of natural formations are neglected. Therefore, geomaterial models and "reservoir-on-a-chip" have been introduced in recent years, in which etched rock,[68] crushed rock grain[69] and mineral coating[55,70,71] are applied in micromodels, respectively. A drawback to current geo-material micromodels is that the wettability between micromodels

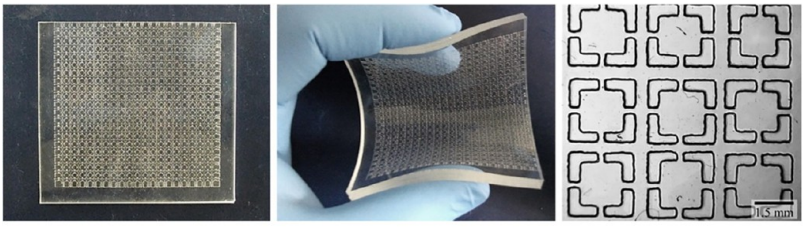

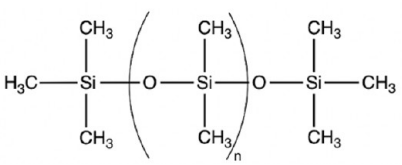

Figure 14. PDMS micromodel and molecular structure of PDMS. Adapted with permission from ref 65. Copyright 2020 Elsevier.

https://doi.org/10.1021/acs.energyfuels.2c01943
Energy Fuels 2022, 36, 9904−9931

Table 2. Summary of Microfluidic Materials

Materials	Elastic modulus	Thermal stability	Fluid compatibility	Fabrication methods	Advantages and disadvantages
Glass	50−90 GPa	500 °C	Compatible to most solvents	Lithography, etching and particle packing	High pressure resistance. Model cost and process depend on fabrication methods.
Silicon	130−180 GPa	1400 °C	Compatible to most solvents	Lithography, etching	High pressure resistance, high resolution. Opaque and expensive.
PDMS	1.32−2.97 MPa	−40 to 150 °C	Incompatible with hydrocarbon, toluene, dichloromethane	Soft lithography, 3D printing	Relatively cheap, easy bonding. Unstable structure.
PMMA	3.1−3.3 GPa	−70 to 100 °C	Incompatible with ethanol, dimethyl sulfoxide, and acetone	Soft lithography, hot embossing, laser engraving, 3D printing	Low cost, good stability. Low resolution and limited fluid compatibility

Table 3. Brief History of Micromodel Development in Oil and Gas Industry[a]

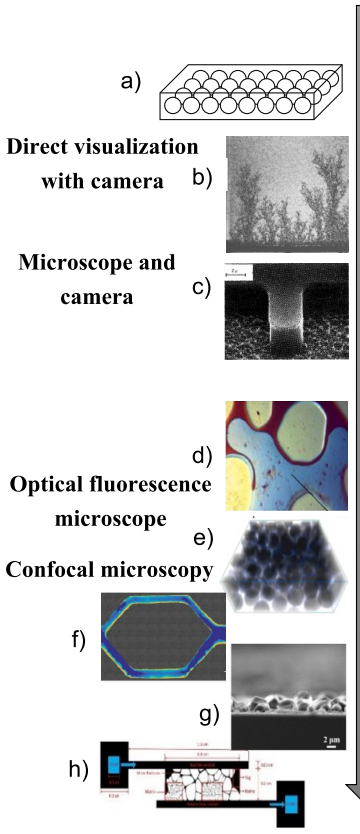

Year	Materials	Fabrication methods	Pore size	Reference
1952	Glass	Pack glass beads in glass cell		73
1957	Glass, sand, plastic etc.	Pack materials sealed by glass	0.5mm	74
1961	Glass	Wax mask, wet etched glass	38μm	75
1978	Silicon	Dry etched silicon substates	2μm	76
1985	Glass	Lithography and chemical etching	10μm	77
1998	PDMS	Soft lithography	30nm	16
1999	PMMA	Hot embossing	0.8μm	34
2005	Epoxy resin	3D printing	3μm	78
2012	Glass	Laser engraving	40μm	79
2015	Section of rock	Laser engraving	250μm	72
2016	Mineral grains	Pack grains in glass channel	200μm	69
2017	$CaCO_3$, glass	In-situ growing CaCO3 in models	250nm	55
2019	Silicon, glass	Thin film deposition	250nm	49

[a]Panel b is reproduced with permission from ref 74. Copyright 1982 Elsevier. Panel c is reproduced with permission from ref 76. Copyright 1979 American Vacuum Society. Panel d is reproduced with permission from ref 79. Copyright 2012 Elsevier. Panel e is adapted with permission from ref 52. Copyright 2013 John Wiley and Sons. Panel f is reproduced with permission from ref 72. Copyright 2015 ROYAL SOCIETY OF CHEMISTRY. Panel g is reproduced with permission from ref 55. Copyright 2017 American Chemical Society. Panel h is reproduced with permission from ref 49. Copyright 2019 ROYAL SOCIETY OF CHEMISTRY.

and the sealing materials is different, which influences fluid flow in micromodels.[72] Besides, it is hard to observe the inside of real 3D micromodels made by geomaterials because they are not transparent to visible light.

4. APPLICATION IN OIL AND GAS RECOVERY

Complex fluid flow in porous media is directly related with oil and gas extraction processes since oil, gas and water must go through porous media. Micro/nanofluidic models have been developed into effective tools to better understand the underlying principles governing how the fluid flow behaves throughout the oil recovery processes since it is challenging to examine the micro/nanoflow behaviors utilizing a core sample at the macroscale only. The first micromodel developed for the oil industry can be dated back to the 1950s.[73] Since then, the micromodel has been widely applied in various oil production process including multiphase flow, EOR and unconventional reservoirs. Here we will show a brief development history of microfluidics (Table 3) and review the applications of micromodels in the oil and gas industry.

From Table 3, it is obvious that the development of microfluidics is based on novel observation techniques, materials and fabrication methods. Specifically, the observation techniques and fabrication methods are aiming to improve

https://doi.org/10.1021/acs.energyfuels.2c01943
Energy Fuels 2022, 36, 9904−9931

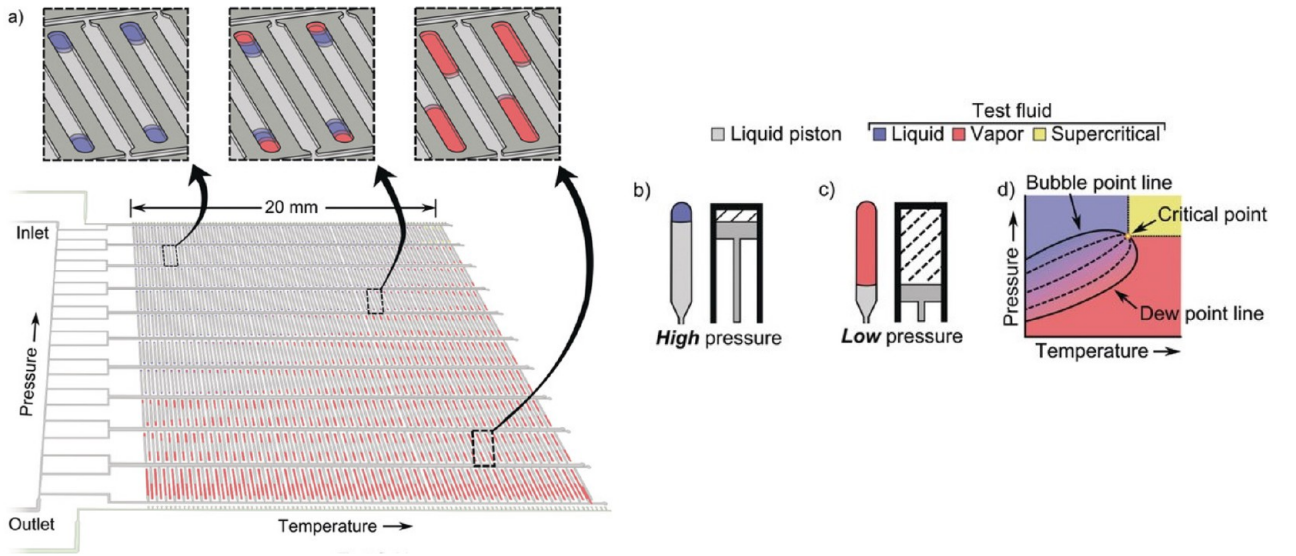

Figure 16. (a) Schematic of the rapid pressure−temperature phase mapping microfluidics. Insets show enlarged regions of the device, Liquid piston operation is demonstrated in panels b and c, respectively. (d) Corresponding phase diagram. Adapted with permission from ref 85. Copyright 2017 John Wiley and Sons.

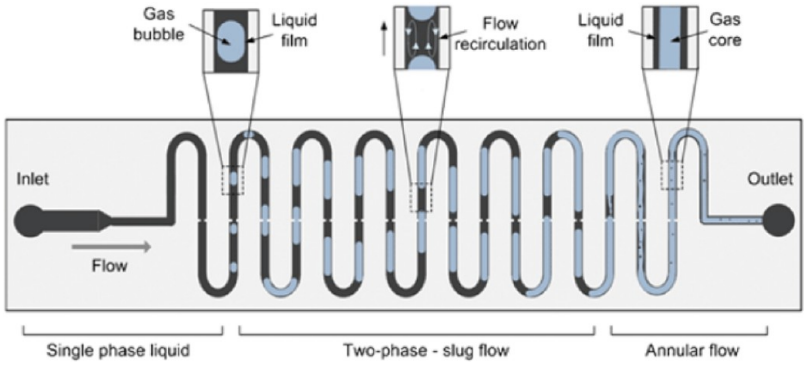

Figure 17. Schematic diagram of two-phase flow in a long serpentine microchannel. Reproduced with permission from ref 86. Copyright 2013 ROYAL SOCIETY OF CHEMISTRY.

resolutions for small pore size. Besides, there has been increasing attention on applying realistic mineralogical compositions in microfluidics in recent years.

4.1. Fluid Characterization. Determination of fluid properties, such as the phase behavior and viscosity, is essential to petroleum engineering, which can be achieved by microfluidics. Compared with conventional pressure−volume−temperature (PVT) cells, microfluidics does not require a large amount of samples for testing, which brings advantages in terms of time and cost. Conventional PVT cells often take several hours to establish the thermal dynamic equilibrium, but microfluidics may achieve thermodynamic equilibrium in minutes or even milliseconds.[80] In addition, it is safer and easier to obtain homogeneous fluid mixtures in micromodels instead of PVT cells. Therefore, micromodels have been used to characterize fluid properties in many experiments.

4.1.1. PVT Analysis. Microfluidics has been a powerful tool to study the phase behavior of fluids. To carry out experiments at a high temperature and pressure, silicon and glass are usually selected to fabricate microfluidics, in which the phase behaviors can be observed directly.[80] Mostowfi et al. first studied the phase behavior of black oil with microfluidics in 2012. They etched a long serpentine microchannel in a silicon substrate and generated an isothermal pressure gradient (at room temperature) in the channel. The local pressure inside the channel was flow-controlled and measured using membrane-based optical pressure sensors positioned along the channel. Although the device could only detect the bubble point of the fluid, the results had an excellent agreement with conventional measurements.[81,82] Pinho et al. enhanced the accuracy of measurement by introducing a dynamic stop-flow mode, making it possible to detect the dew point at a constant pressure and different temperatures in the system.[83] Bao et al. presented the direct measurement and observation of the full pressure−temperature phase diagram in microfluidics, in which orthogonal, linear, pressure and temperature gradients are obtained with 100 parallel microchannels. Pressure control was achieved by a pressure gradient caused by fluid flow in the channel, and temperature was controlled by a heater and a cooler. The method allows us to observe 10 000 individual results, each at a distinct pressure and temperature.[84] Xu et al. extended the method to 1000 chambers, each isolated by a liquid piston and set to a different pressure and temperature combination (Figure 16), allowing the microfluidics to show a full PVT diagram of the hydrocarbon mixture at once.[85] The phase behavior at the nano-scale was also investigated by nanofluidics in recent years.

https://doi.org/10.1021/acs.energyfuels.2c01943
Energy Fuels 2022, 36, 9904−9931

4.1.2. Solubility and Diffusivity. The gas−oil ratio, wax and asphaltene precipitation are major concerns during production, transportation and processing of hydrocarbons, which can be studied in microfluidics. Fisher et al. measured the gas−oil ratio of live oil (crude oil with dissolved gas) after flowing through a serpentine microchannel (Figure 17), which was analogous to the production of crude oil from a formation. The liquid and gas volume were collected in a liquid trap and gas meter. They showed excellent agreement with the gas−oil ratio obtained from conventional methods.[86] Molla et al. calculated the gas volume in a long serpentine microchannel by measurement of liquid and gas slug length locally, and they provided a measurement over a wide range of pressures.[87] In 2016, Molla et al. also measured the wax precipitation temperature of normal alkanes, binary mixtures and multicomponent crude oil by monitoring the flowing pressure increase in similar microfluidics (Figure 18).[88] Schneider et al.

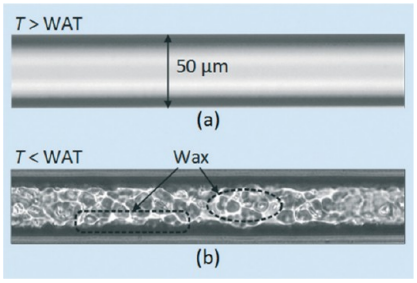

Figure 18. Observation of wax appearance of oil in the microchannel, when (a) temperature is above the wax appearance temperature (WAT) and (b) below the WAT. Reproduced with permission from ref 88. Copyright 2016 ROYAL SOCIETY OF CHEMISTRY.

presented microfluidics (Figure 19), a multilayered micromodel fabricated by lithography, for the measurement of asphaltene content based on linear absorption in UV−vis spectroscopy. Compared with conventional gravimetric techniques, it only took less than 30 min to obtain the results.[89] Hu et al. investigated deposition of asphaltenes in a quartz-packed microfluidics, which was made of silicon and Pyrex wafers by lithography. The solubility of asphaltenes in hydrocarbons was measured by its absorbance in UV−vis spectroscopy. They found larger Reynolds number caused less asphaltenes precipitation in porous media.[90] Qi et al. fabricated a 2D silicon-glass microfluidics by a deep reactive ion etching method and they quantified the asphaltene deposition rates for *n*-pentane and *n*-heptane with fluorescence microscopy with a Fourier transform infrared (FTIR) filter cube. According to their results, heavier fractions and aromatic/naphthenic components generated less asphaltenes and exhibited a slower deposition rate, resulting in less pore damage and overall better performance.[91]

For carbon capture, utilization and storage, areas where microfluidics have attracted growing interest in recent years, the solubility and diffusivity of CO_2 in crude oil is essential. Fadaei et al. first presented a cross-channel glass microfluidic to study CO_2 diffusion in bitumen. Based on one dimension bitumen swelling measurement and a mathematical model, they calculated the diffusion coefficients of CO_2 in bitumen for different pressures, which was in good agreement with the relevant published data using conventional methods.[92] Sell et al. quantified CO_2 diffusion in brine by a pH dependent dye in microchannels. In their work, CO_2 diffusivity measurement was achieved in less than 90 s, keeping good accuracy, which was much faster than conventional methods.[93] Similar with PVT analysis, the minimum miscibility pressure (MMP) of CO_2 can be investigated by microfluidics. Nguyen et al. quantified the MMP of CO_2 in crude oil by a fluorescent microscope and microfluidics, which was fabricated through deep reactive ion etching of silicon (Figure 20). Compared to conventional methods, the results differed by less than 0.5 MPa on average.[94] In 2018, Sharbatian et al. developed a microfluidics that was able to characterize solubility, diffusivity, extraction pressure, miscibility and contact angle. The microfluidics was played as a platform to obtain comprehensive fluid properites.[95]

In addition to PVT analysis, solubility and diffusivity measurement, microfluidics can also be used to determine viscosity[96−98] and density.[99,100] However, these applications are challenging and not widely used in the oil and gas industry

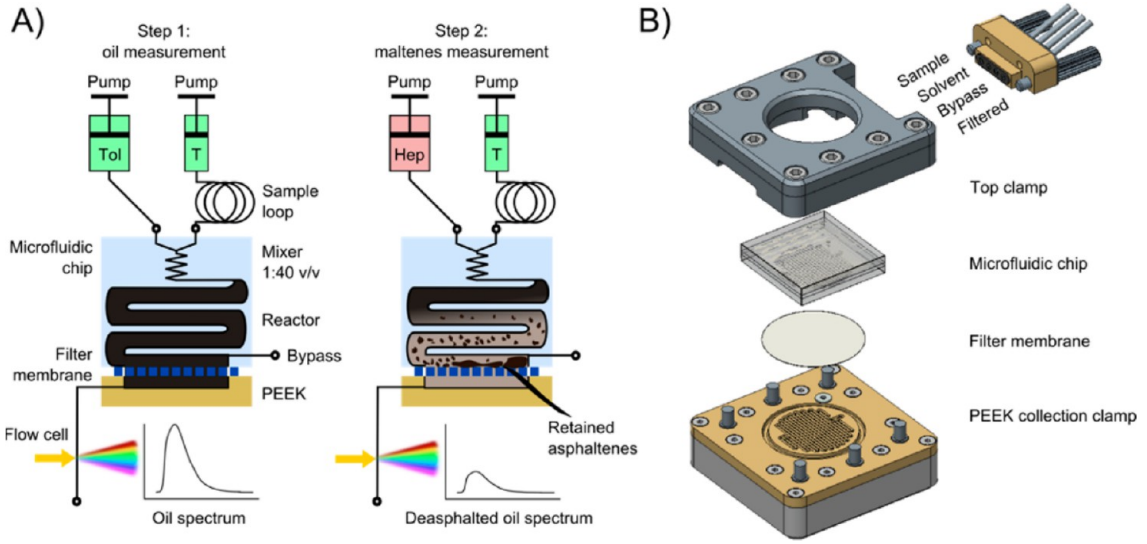

Figure 19. (A) Concept and flow diagram. (B) Enlarged view of the chip assembly. Reproduced with permission from ref 89. Copyright 2013 American Chemical Society.

https://doi.org/10.1021/acs.energyfuels.2c01943
Energy Fuels 2022, 36, 9904−9931

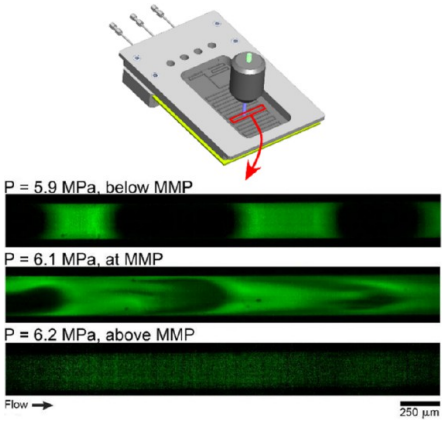

Figure 20. Microfluidics to measure minimum miscibility pressure. Reproduced with permission from ref 94. Copyright 2015 American Chemical Society.

since the flow rate inside the microchannel is in a very limited range.[80]

4.2. Multiphase Flow. Multiphase flow in porous media is important in the oil recovery process, including waterflooding and EOR, and it is determined by pore geometry, pore surface characteristics, fluid properties, fluid–fluid interactions and rock–fluid interactions. Understanding multiphase flow is of importance to study displacement efficiency, water breakthrough and remaining and residual oil distributions. A micro/nanomodel has been applied to study the effects of capillary number, wettability and porous media type (heterogeneity and well patterns) on flow pattern, shape and distribution of the trapping phase, and numerical models of two-phase flow can be corrected and validated by micromodels.

4.2.1. Flow Pattern and Capillary Number. The Hele–Shaw cell, the early micromodel to study two-phase flow (oil and water) in 1952, is a very simple model made of two parallel transparent plates, with the flow in the glass-beads matrix between plates, in which a fingering phenomenon and residual oil formation were observed and discussed.[73] The limitation is that it is a 2D model and the visualization results could not be recorded at that time. Zhao et al. fabricated 2D circular micromodels with NOA81 to conduct radial fluid displacement. They varied a series of capillary numbers and wettability in the experiments to investigate displacement patterns and flow patterns as shown in Figure 21.[101] Krummel et al. built a glass-beads model that can have a real 3D pore structure (Figure 11). In their experiments, confocal microscopy is utilized to visualize the pore-scale dynamics of ganglion formation and trapping, and to characterize the intricate structure of the trapped ganglia.[52] Datta et al. used the same experimental setup proving that capillary number plays an important role in the unstable flow pattern in two-phase flow.[102] It is also suggested by Cottin et al. that capillary number is the key controlling the transition from capillary flow to viscous flow.[103]

4.2.2. Wettability. In addition to the capillary number effect, the wettability effect on fluid flow behavior was also investigated using a micromodel of which the wettability can be designed. Maaref et al. fabricated 2D etched glass models and compared intermediate wet and oil wet in the waterflooding process, concluding that intermediated wetting contributed to more oil recovery.[104] The distribution of wettability of the micromodel can also be designed. To have micromodels with spatial wettability heterogeneities at the pore level, Schneider et al. combined the soft lithography of PDMS with hydrophilic poly(acrylic acid) that is adhered in the small pores (Figure 22). They claimed that wettability

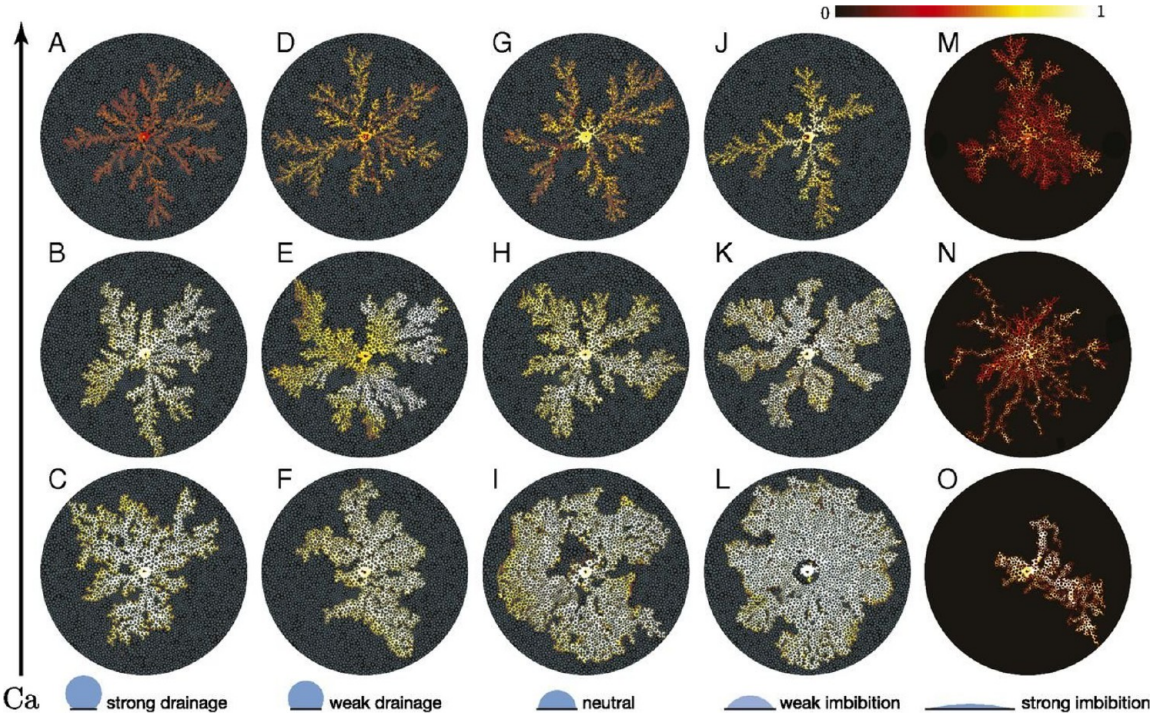

Figure 21. Displacement patterns of different capillary number and wettability condition, the colormap shows the saturation of the invading water. Reproduced with permission from ref 101

https://doi.org/10.1021/acs.energyfuels.2c01943
Energy Fuels 2022, 36, 9904–9931

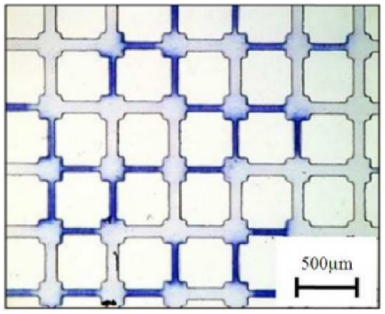

Figure 22. Mixed wet PDMS micromodel (hydrophilic surface is blue). Reproduced with permission from ref 105. Copyright 2011 Science Publications.

heterogeneity led to different residual oil saturations and injection pressures.[105] Besides, the contact angle of the micromodel can be controlled by various methods, including chemical vapor deposition and UV treatment.[106] Zhao et al. demonstrated the existence of a critical wetting transition that controlled pore-scale flow by varying wettability using chemical vapor deposition.[101]

4.2.3. Trapping Phase. The trapping phase in a multiphase flow is of importance in oil recovery, which can be studied in micromodels. The formation, volume, shape and distribution of the trapping phase can be easily observed and calculated (Figure 23). In the early 1980s, Chatzis et al. performed experiments in capillary models and identified bypass trapping and snap-off trapping.[107] Xu et al. found the 2.5D model was better for the phase trapping study as residual oil was observed while some 2D models did not have such a phenomenon.[22] The residual oil distribution and type can be visualized in micromodels with different pore structures (different pore shapes,[108] double channels,[1] and fracture model,[4] wettability[109]) and fluid properties.[110] Besides, Tian et al. observed the formation process of trapped water in gas−water flow using 2D glass micromodels.[111]

4.2.4. Three-Phase Flow. Three-phase (gas−liquid−liquid) flow has attracted interest in micromodels in recent years. Wang et al. observed flow patterns in a cross-junction microchannel device and introduced a new capillary number and six flow modes to distinguish the complicated three-phase flow.[112] Yue et al. extended a two-phase pressure drop model under a slug to obtain a three-phase slug flow model in a long channel.[2] Porter et al. developed a silicon micromodel that allows for direct observations of three-phase immiscible/miscible displacement and oil recovery of CO_2, *n*-decane and brine, respectively (Figure 24).[72] The pressure and temperature of the micromodel experiments were 8.3 MPa and 45 °C,

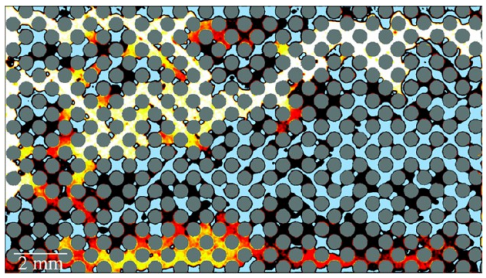

Figure 24. Supercritical CO_2 (white) displacing *n*-decane (black) and brine (blue). Reproduced with permission from ref 72. Copyright 2015 ROYAL SOCIETY OF CHEMISTRY.

respectively. Three-phase flow may occur in the CO_2 Huff-n-Puff process. Lu et al. visualized water−oil−CO_2 flow by the micro-Particle Image Velocimetry method in a silicon-glass micromodel. They found that the exsolution induced CO_2 bubbles in aqueous and oil phase blocked the preferential migration passage and dominated different multiphase migration mechanisms under different wettabilities.[113]

4.2.5. Numerical Simulation. Finally, the experimental results of multiphase flow in micromodels are combined with numerical simulations. The availability of microfluidics to characterize the pore space with a high level of detail fosters the growing interests in pore-scale modeling. Many pore-scale modeling methods have been widely used by researchers to study fluid displacement in porous media, including the lattice Boltzmann method (LBM), smoothed particle hydrodynamics (SPH), volume of fluid (VOF) method, pore network modeling, and statistical models.[104,114] Liu et al. developed a color-gradient LBM to simulate spontaneous imbibition in a porous media, and it was validated in an etched silicon micromodel.[115] Tian et al. used a 2D glass micromodel to obtain the effects of geometry and wettability on waterflooding, and they developed a multicomponent LBM model to simulate the results.[116] Bandara et al. used SPH to model the immiscible flow in a micromodel.[117] They simulated flow for a wide range of capillary numbers and viscosity ratios, validated by the results in a 2D dry etched model by Zhang et al.[118] Jung et al. combined Hele−Shaw cell with particle-based simulations finding a consistent crossover between stable displacement and fingering.[119] Ferrari et al. presented a detailed comparison of pore-scale simulations and experiments

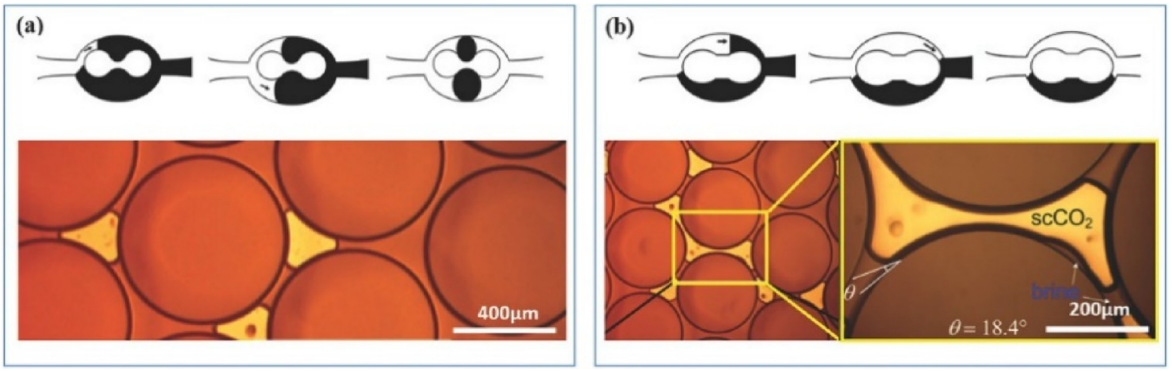

Figure 23. (a) By-pass trapping phase and (b) snap-off trapping phase. Reproduced with permission from ref 10. Copyright 2018 Small.

https://doi.org/10.1021/acs.energyfuels.2c01943
Energy Fuels 2022, 36, 9904−9931

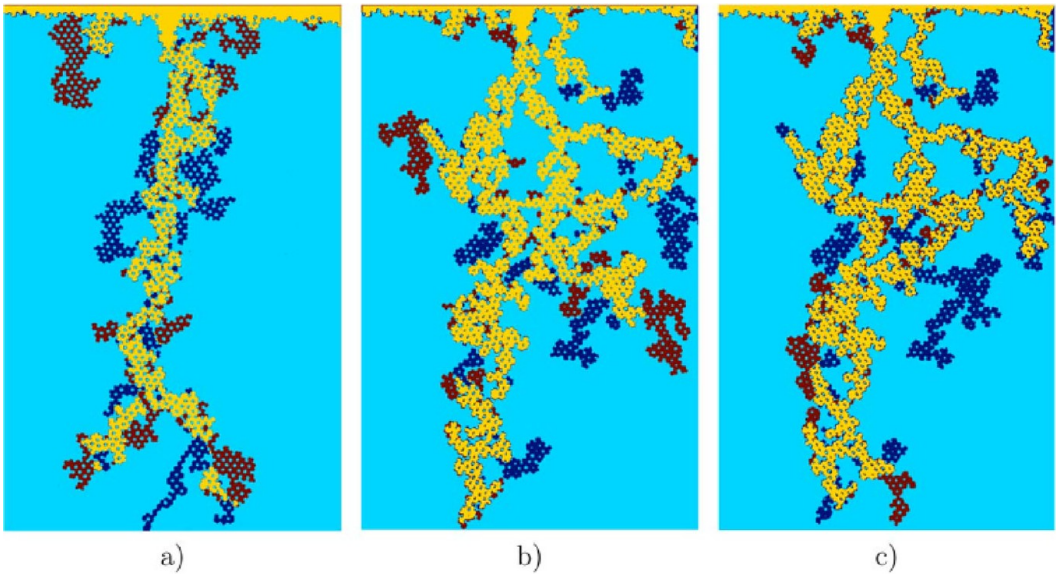

Figure 25. Comparison between simulation and experiment results. Yellow area represents the successful simulation. (a) Homogeneous geometry; (b) heterogeneous geometry; (c) heterogeneous 3D model. Reproduced with permission from ref 120. Copyright 2015 John Wiley and Sons.

for unstable primary drainage in Hele−Shaw cells, by solving the Navier−Stokes equations and employing the VOF method to track the evolution of the interface (Figure 25).[120] Niasar et al. developed an unstructured pore network model to simulate experimental results of drainage and imbibition that was performed on a two-dimensional micromodel. According to their conclusion, the simulation is able to reproduce the distribution of the fluids as observed in the micromodel experiments.[121]

4.3. Enhanced Oil Recovery. Enhanced oil recovery (EOR) is a broad range of processes that aim to improve oil recovery, which is usually accompanied by flow and transport of chemicals, phase behaviors and chemical reactions in porous media. Micro/nanofluidics can serve as better candidates for assessing EOR processes than conventional coreflooding tests in real-time visualization and exploration of mechanisms, such as low-salinity water, polymer, surfactant, alkaline, nanoparticle, in-situ gel, preformed particle gel, foam, thermal methods and microbial.

4.3.1. Low-Salinity Water. Low-salinity water flooding (LSW), or smart water flooding, is defined as recovery techniques aiming at improving recovery by reducing and/or modifying the ionic content of injected brines.[122] Wettability alteration in an oil−brine−rock system is one of the major EOR mechanisms for LSW. Shaik et al. visualized and characterized solid−fluid interactions by changing salinity, divalent cations and temperature in a $CaCO_3$-coated glass channel.[123] Bartels et al. stated that wettability alteration was a necessary but not sufficient requirement for incremental recovery by LSW, as they observed the release of oil drop in micromodels with deposited clay.[124] During LSW flooding, clay particles could be detached in the presence of low-salinity brine, resulting a blockage of pores and alteration of wettability. Song et al. fabricated a silicon micromodel coated with kaolinite and found the release of kaolinite particles at pore level in response to changes in brine concentration (Figure 26).[125] In addition, Li et al. found that LSW could invade the pores that were inaccessible by high-salinity water in a quartz-filled 2D model, and they suggested that sweep efficiency improvement was due to wettability alteration.[126] In addition, Morishita et al. claimed that emulsions caused by LSW should be an important factor since they visualized the pore blockage and microwater dispersion phenomena of emulsion that contributed to oil recovery during LSW flooding.[127] Although low-salinity waterflooding is a cooperative process in which multiple mechanisms acting on different length and time scales, micromodels have attracted increasing attention in LSW studies.[122,128−130]

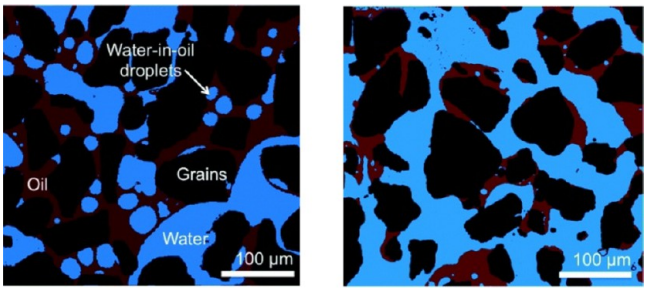

Figure 26. Micromodel after high-salinity flood (left) and after low-salinity flood (right). Adapted with permission from ref 125. Copyright 2015 ROYAL SOCIETY OF CHEMISTRY.

4.3.2. Polymer Flooding. Polymer flooding is one of the most favorable and applied EOR methods in oilfields.[131] The main EOR mechanism of polymer flooding is mobility ratio improvement and resultant sweep efficiency improvement. However, there is a long debate regarding whether these viscoelastic polymer solutions reduce residual oil saturation. Micromodels have been used to study the polymer behaviors and explore underlying EOR mechanisms. For example, Wegner et al. injected a polymer to displace residual oil after waterflooding in a 2D dry-etched silicon model. They found that the polymer did not show a significant increase in oil recovery due to viscoelasticity.[132] Meybodi et al. carried out oil displacement experiments at varying conditions of flow rate, water salinity, polymer type and concentration in five-spot glass micromodels, investigating how local and global heterogeneity control polymer flooding.[133] In addition to sweep efficiency improvement, the viscoelasticity of polymer

https://doi.org/10.1021/acs.energyfuels.2c01943
Energy Fuels 2022, 36, 9904−9931

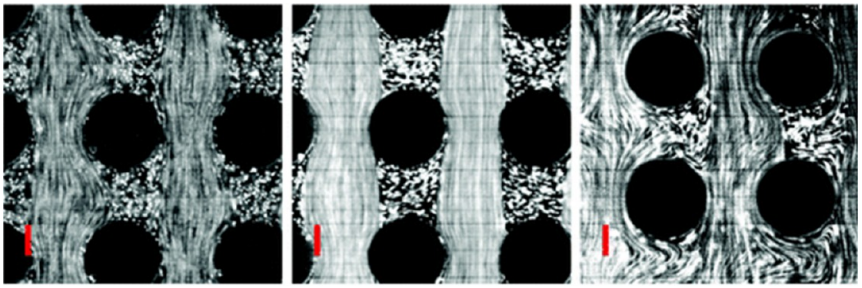

Figure 27. Streamline snapshots of the flow at stable flow (left), onset of elastic instability (middle) and high shear rate (right). Adapted with permission from ref 134. Copyright 2017 ROYAL SOCIETY OF CHEMISTRY.

increases the viscous forces, and the turbulent elastic flow could mobilize a higher amount of oil through dead-end pores, which is confirmed in some microfluidic experiments. Kawale et al. measured the pressure-drop and visualized the flow field in PDMS micromodels made by soft lithography. They directly validated the elastic instability with respect to the pressure build-up and investigated the pore-shape effects (Figure 27).[134] The pulling effect of a viscoelastic polymer solution can lead to carrying out of residual oil in the dead end of pores. Wang et al. observed that some of residual oil in a wedge-shaped hole was displaced in a water-wet glass etched model.[135]

Polymer flooding is limited by degradation and retention of polymer chains. Dupas et al. studied mechanical degradation of water-soluble polymers using a capillary device and showed how mechanical extension of polymer chains affected performance of a polymer flooding.[136] Sugar et al. observed polymer retention in a 2D PDMS micromodel and presented three retention mechanisms of polymer. Yun et al. investigated polymer retention with an etched silicon model, and they developed a new image-based technique for direct visualization and quantification of polymer retention.[137]

4.3.3. Surfactant. Adding a surfactant can dramatically decrease the interfacial tension between oil and water, resulting in an increased capillary number and a decreased residual oil saturation in porous media.[138] The technique is often combined with other chemical injection, such as polymer and alkaline. Micromodels have advantages over conventional core flooding tests in real-time contact angle measurement, observation of emulsification and detection of residual oil. The oil recovery in a fractured reservoir by surfactant flooding is mainly dependent on the imbibition of the surfactant solution into the matrix.[139] Yu et al. incorporated the 3D geometry of rock into a 2.5D micromodel. Imbibition of a Winsor I type surfactant system was investigated, accompanied by explanation and visualization of two EOR mechanisms, namely microemulsion imbibition and residual oil solubilization.[140] They also found that there was a competitive relationship between the wettability alteration and emulsification.[141] Zhao et al. injected surfactant in homogeneous and heterogeneous glass-etched micromodels, and they found both oil-in-water (O/W) and water-in-oil (W/O) emulsions in micromodels during the surfactant flooding (Figure 28).[142] Mohammadi et al. conducted surfactant flooding in both homogeneous micromodel and micromodel with flow barriers. The experimental results showed that surfactant solution led to the mobilization and coalescence of trapped oil droplets.[143] Yang et al. investigated surfactant flooding at the pore-scale by using a 2.5D glass micromodel, and they revealed the effects of

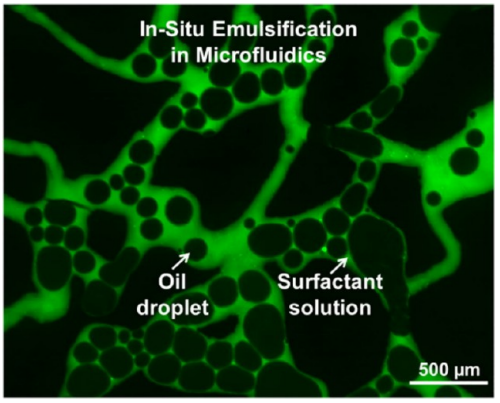

Figure 28. In-situ emulsification in microfluidics. Reproduced with permission from ref 142. Copyright 2020 Elsevier.

dynamic contact angle on the ultralow interfacial tension (IFT) displacement.[144]

4.3.4. Alkaline. Reducing IFT and changing the wettability, alkaline improves oil recovery by producing in-situ surfactants from the reaction between alkaline and the acidic crude oil. Using 2D glass model, Dong et al. investigated two EOR mechanisms of alkaline flooding in heavy oil: in-situ water-in-oil emulsion formation with wettability alteration and oil-in-water emulsion formation.[145] Pei et al. also conducted alkaline injection to enhance heavy oil recovery in a 2D glass micromodel and they concluded that formation of a water-in-oil (W/O) emulsion reduced the mobility of the water phase and diverted the injected water into the unswept region.[146] Alkaline is often used with combination of other methods, such as alkaline–surfactant–polymer (ASP). Using micromodels, the sweep efficiency can be observed clearly as shown in Figure 29. Alzahid et al. conducted alkaline–surfactant and alkali–surfactant–polymer flooding in PDMS micromodels and they presented micro-scale images of these two formulations, studying displacement mechanisms and pore-scale emulsion.[147] Nie et al. also conducted ASP flooding in 2D glass models with different pore size distribution. They claimed that increasing the viscosity of the injection fluid showed a negative impact on improving the oil recovery ratio because the mobilization of residual oil in smaller pores was greatly impacted by emulsification.[148]

4.3.5. Nanoparticle. The EOR mechanisms of nanoparticles include disjoining pressure, interfacial tension reduction, wettability alteration and sweep efficiency improvement.[150] Although nanoparticles have been developed for EOR fields, there are debates regarding their transport ability and EOR mechanisms. To explore the potential application of nano-

https://doi.org/10.1021/acs.energyfuels.2c01943
Energy Fuels 2022, 36, 9904–9931

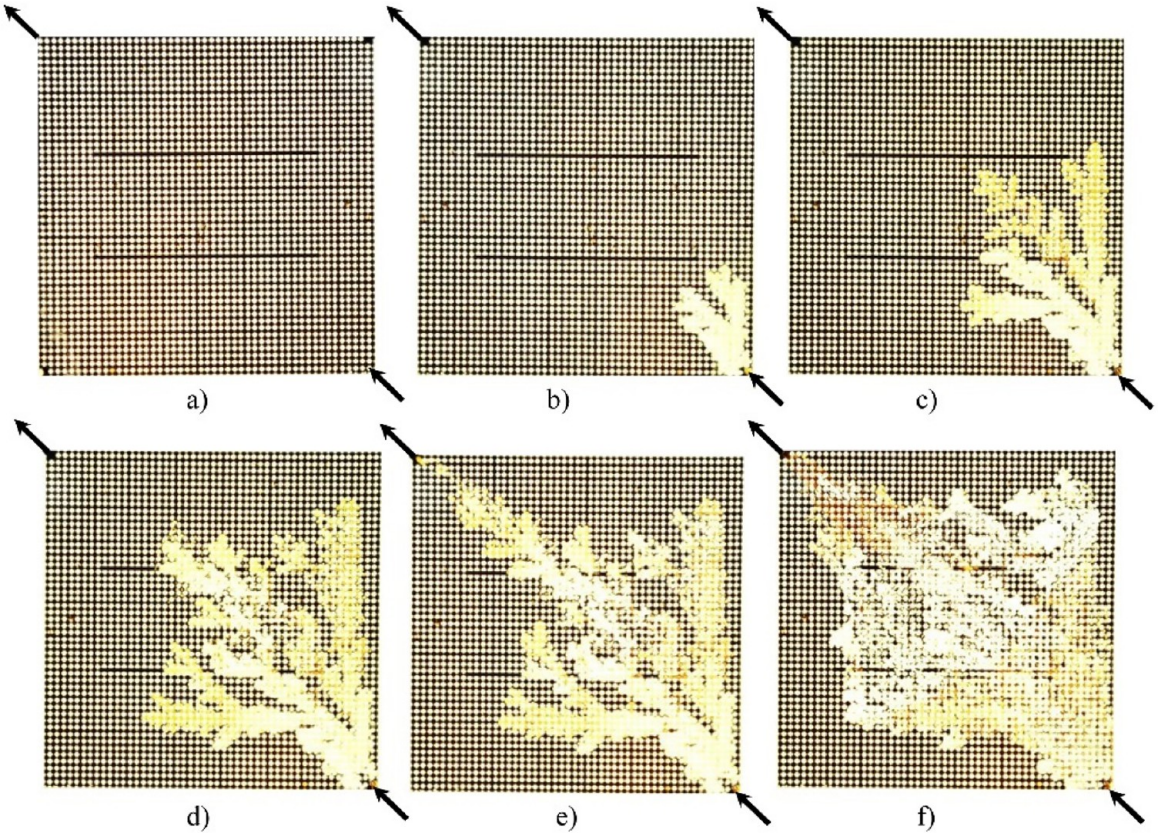

Figure 29. Propagation of the ASP phase in a laser engraving glass micromodel. Reproduced with permission from ref. #149. Copyright 2016 John Wiley and Sons.

particles, micromodels have been widely used in recent years since these EOR mechanisms are at the micro/nano-scales. Rostami et al. fabricated a 2D glass micromodel by laser engraving and they injected silica nanoparticles to displace oil. According to the observation of a thin oil film formation at the pore-scale, they attributed the phenomenon to disjoining pressure.[151] Li et al. prepared a 2D silicon micromodel by dry etching, and they compared silica-based nanofluid with conventional water on the performance of oil displacement in the micromodel. After measurement of the contact angle and residual oil saturation, they suggested that wettability alteration was the dominating EOR mechanism rather than the interfacial tension (Figure 30).[152] Retention of nanoparticles is a concern of application in oilfields. Hendraningrat et al. investigated interfacial tension reduction, nanoparticles retention and permeability impairment in glass micromodels. Based on microscopic visualization of the glass micromodel, they found that nanoparticles deposited and adsorbed at surface pore network and resultant plugging efficiency ranged from 41% to 72%.[153] In addition, nanoparticles can be combined with other techniques, such as surfactant[154] and water alternating gas flooding (WAG),[155] which are also investigated by micromodels. What is more, nanoparticle transport is essential for its application. There are many colloid transport experiments and models since it is also important in other engineering issues. In terms of the oil and gas field, Suzuki et al. used dry-etched silicon micromodels to visualize particle transport in fractured porous media. Tunable resistive pulse sensing was used to measure the frequency distributions of particle diameters from the effluent. They suggested that tracer response of micro/nanoparticles might be useful to evaluate the fracture structures and the flow properties for different flow pathways.[3]

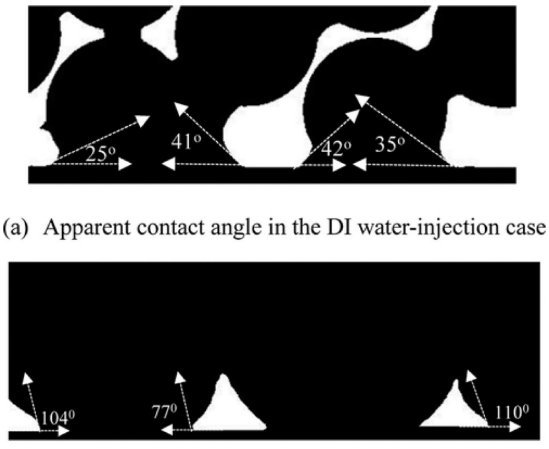

Figure 30. Contact angle measurement in a micromodel. Reproduced with permission from ref 152. Copyright 2017 American Chemical Society.

4.3.6. In-Situ Gel. Gel treatment is a very popular conformance control method by which a large number of oilfields have improved sweep efficiency.[156] Gel performance under different geometries and fluids can be evaluated and visualized in micromodels. Hasankhani et al. injected in-situ polymer gels into 2D glass models with different fracture directions, in which oil recovery was calculated through an

https://doi.org/10.1021/acs.energyfuels.2c01943
Energy Fuels 2022, 36, 9904−9931

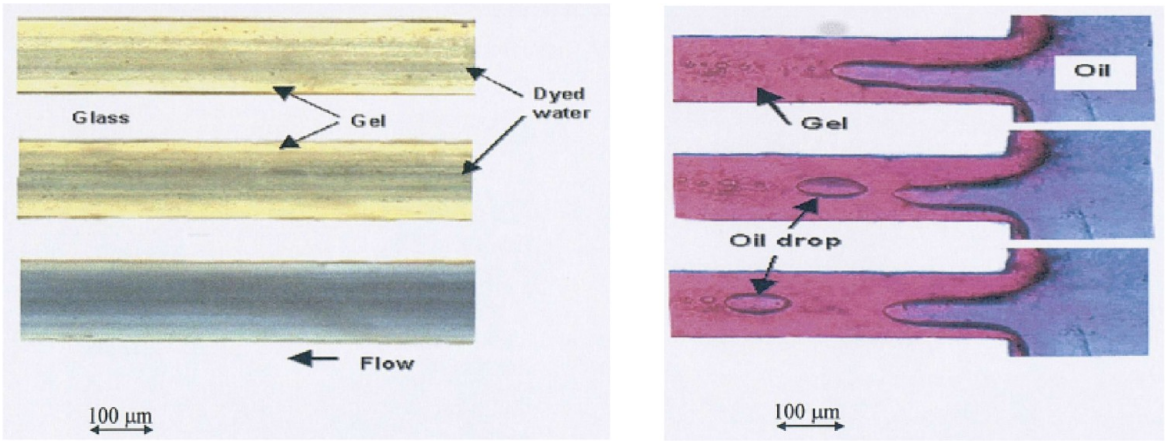

Figure 31. Dyed water in gel matrix (yellow) was displaced by brine (blue), and oil flow through gel matrix. Adapted with permission from ref 159. Copyright 2000 Imperial College London.

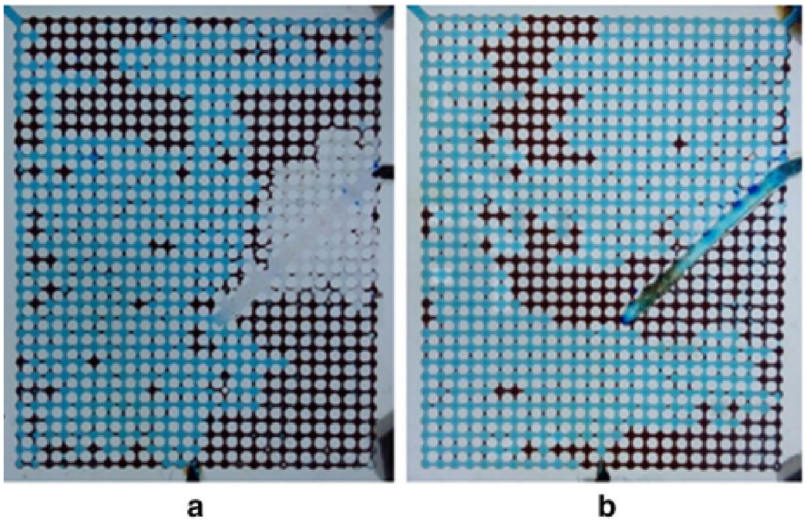

Figure 32. Oil distribution after gel treatment and waterflooding (oil phase is black, water phase is blue). (a) In-situ gel treatment and (b) PPG treatment. Reproduced with permission from ref 165. Copyright 2019 Springer Nature.

image analysis technique. According to their visualization results, the asphaltene-augmented gel polymer system has a better performance than the conventional gel system. It can be observed very clearly that the fracture direction in micromodels influences sweep efficiency.[157] Al-Sharji compared water flow and oil flow in a capillary that was filled with a polymer gel. He showed that water flowed through the gel matrix in a "diffusive" manner, as if flowing through a porous medium, whereas the oil pushed its way through the gel in the form of immiscible drops or filament (Figure 31).[158,159] Liang et al. also obtained the similar results when they investigated disproportionate permeability reduction of the polymer gel. They suggested that the gel-displacement mechanism was a primary reason for the development of the oil flow path. They also showed the expansion of the oil path because of gel dehydration.[160]

4.3.7. Preformed Particle Gel. In addition to a conventional in-situ polymer gel, preformed particle gel (PPG) is another type of gel that has drawn increasing attention recently. PPG can be injected when there are fractures and extremely high permeability channels.[161] Bai et al. first applied an etched glass micromodel to study the transport pattern of PPG in porous media. They proposed six PPG propagation patterns and demonstrated that a PPG particle could deform and pass through a pore throat with a diameter that was smaller than the particle diameter because of its elasticity and deformability.[162] Zhang et al. constructed transparent fracture models. They found that PPG transported along fractures like a piston movement and a gel pack was formed in the fracture; water channels were formed when water broke through the gel pack.[163] Aqcheli et al. injected PPG to displace oil in a 2D glass micromodel, and they used image analysis software (ImageJ) to calculate the oil recovery. The microscopic images after the injection of PPG showed that it could sweep the oil trapped in the micromodel with a higher sweep efficiency.[164] Heidari et al. injected in-situ and PPG into the micromodels with several different geometries to compare their ability in blocking fractures and increasing the oil recovery. They claimed that PPGs were more successful to resist salt water and recovery of trapped oil in their micromodels (Figure 32).[165] Moreover, swelling behaviors of PPG in porous media can be directly visualized. Louf et al. directly visualized the swelling of hydrogels confined in three-dimensional granular media and demonstrated that the extent of hydrogel swelling was determined by competition between swelling force by gel particle and confining force by surrounding (Figure 33).[166]

https://doi.org/10.1021/acs.energyfuels.2c01943
Energy Fuels 2022, 36, 9904−9931

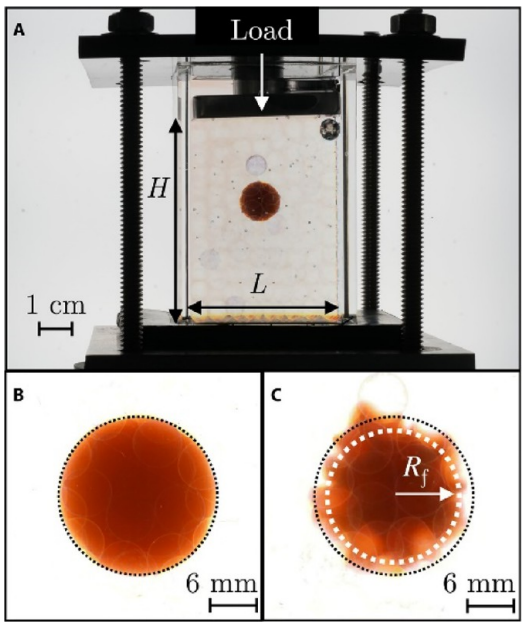

Figure 33. (A) Apparatus for testing hydrogel swelling in confinement. (B) Image of a hydrogel swollen within a medium without load. (C) Image of a hydrogel swollen within a medium under a strong applied load. Reproduced with permission from ref 166. Copyright 2021 American Association for the Advancement of Science.

Polymer micro/nanogels, which are developed based on PPG techniques, have attracted a lot of interest in the EOR field. In the size of micro/nanometers, these gel particles are designed to be conformance control agents for in-depth fluid diversion, and various experimental research has been undertaken to investigate the possibilities of applying micro/nanogels in oilfields.[167] A simple geometry, such as a capillary tube, can be used to analyze the transport of a particle.[168−171] Li et al. synthesized a microgel with a controlled diameter and elastic modulus by microfluidics. They correlated the injection pressure and particle size, channel size and particle elasticity when a single microgel was transported in a straight confining channel.[172] They also proposed a generalized capillary bundle model to quantitively study the injection pressure of the microgel.[173] Besides, flow pattern and retention can be studied by a micromodel. Yao et al. built a transparent sandpack micromodel that was used to observe the microscopic retention and oil displacement (Figure 34 left).[174] Zhang et al. packed 3D glass-beads micromodels and they used confocal microscopy to observe flow pattern and flow stream, confirming that the nanogel can redirect the flow.[175] Zhang et al. visualized the flow of fluorescent nanogel in 3D glass-beads micromodels. By injection of the nanogel to displace oil, they observed small Pickering oil-in-water emulsion, showing the emulsification ability of the nanogel (Figure 34 right).[176]

4.3.8. Foam. Foam is defined as a gas dispersion within a continuous liquid phase. An individual gas bubble is separated by thin liquid films, stabilized by surfactants at the gas/liquid interfaces.[177] Foam is a remediation of gas breakthrough when the mobility ratio of oil to gas is too high since it can reduce gas mobility. This area focuses on the stability mechanisms of foam flow at the pore level, where micromodels contribute significantly. Foam instability in an open system is dominated by three interdependent processes, drainage, coalescence and coarsening.[178] Jiménez et al. gave both a qualitative and quantitative description of foam flowing through an etched micromodel and foam flowing through a periodically narrowing pore. They proposed foam stability parameters were based on the velocity of the foam flow.[179] Almajid et al. used etched silicon micromodels to observe foam generation and coalescence processes at the pore level in the presence of oil, and they found a new mechanism, called hindered generation.[63] Jones et al. used a borosilicate-glass 2D micromodel and recorded foam coarsening by time-lapse photography. Monitoring the bubble size evolution and the positions of the bubble films, three coarsening regimes were observed in the micromodel experiments (Figure 35).[180] Gauteplass et al. fabricated 2D etched silicon micromodels by considering grain shape, grain size and aspect ratios from thin-section analysis of sandstone. They found that foam injection in layered media successfully diverted gas from a high permeable fracture to a low permeable matrix.[181] Nanoparticle induced foam,[182,183] polymer enhanced foam[184] and self-generated heat foam[185] were also investigated by 2D glass micromodels.

4.3.9. Heavy Oil Recovery. Enhanced oil recovery from heavy oil reservoirs has significantly increased with the increasing demand of energy. As we mentioned, extraction of heavy oil by alkaline flooding was studied using a micromodel etched into the glass substrate.[145,186−188] In addition to alkaline, steam assisted gravity drainage (SAGD) and a light carbon solvent are able to enhance heavy oil recovery, of which the main idea is to reduce the viscosity of heavy oil. In the SAGD, two horizontal wells are drilled parallel to each other and are completed near the base of the pay zone with a vertical spacing of 5−7 m from each other. The upper well injects steam at a constant injection pressure, while the lower production well produces water condensate and draining mobile oil.[11] Mohammadzadeh et al. fabricated an inverted-bell vacuum chamber to minimize the excessive heat loss when

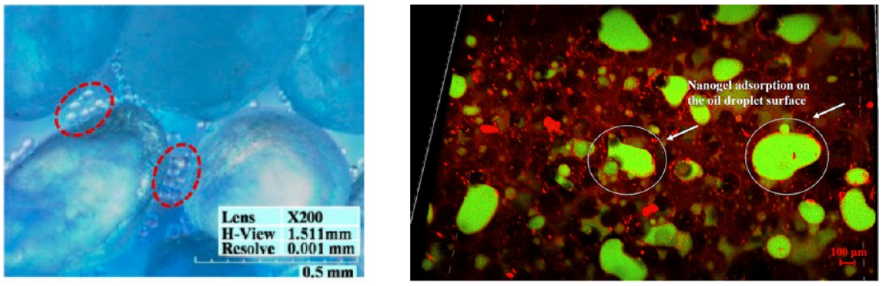

Figure 34. Microgel retention (left). Reproduced with permission ref 174. Copyright 2015 American Chemical Society. Pickering emulsion by nanogel with oil in green and nanogel/fluid in red (right). Reproduced with permission from ref 176. Copyright 2021 American Chemical Society.

https://doi.org/10.1021/acs.energyfuels.2c01943
Energy Fuels 2022, 36, 9904−9931

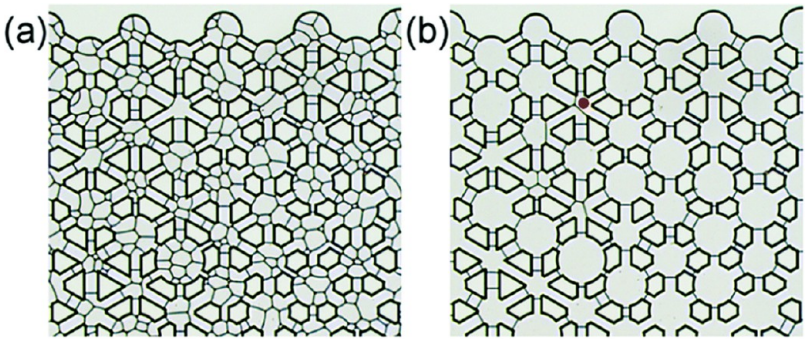

Figure 35. (a) Before coarsening of foam and (b) after coarsening in micromodel. Reproduced with permission from ref 180. Copyright 2018 ROYAL SOCIETY OF CHEMISTRY.

steam was injected. Under different superheating levels, local temperatures in micromodels were recorded in real-time and the overall steam consumption to produce one unit of the mobile oil was corrected based on the heat loss analysis.[189] de Hass et al. fabricated glass micromodels with etched pillar array to mimic sand grains in reservoir, and steam was injected into the chip. They visualized and quantified the oil recovery dynamics in real-time, comparing efficiencies of oil recovery using steam and steam with alkaline additive.[190]

The diffusion coefficient of a solvent in heavy oil is a key to determine how effective the solvent-aided method is. Zhao et al. fabricated a silicon micromodel by dry etching, and diffusion tests were performed at temperatures ranging from 20 to 120 °C and pressures up to 100 bar. The diffusion coefficient was calculated by processing a fluorescence light intensity image.[191] In these investigations using the thermal technique, temperature control and monitoring in the micromodel are crucial components. Karadimitriou et al. developed the visualization setup, with a thermal camera and an optical camera, which could monitor and record the distribution of fluids and their thermal signature. Their results can explain the kinetic heat transfer during multiphase flow in porous media.[192] Light hydrocarbon solvents can be used in bitumen extraction. Qi et al. constructed a 2D glass model by wet etching, which could resist high-pressure high-temperature with a reservoir-relevant geometry. They claimed that liquid propane produced larger emulsions with some mobility after comparing propane and butane at the interface, pore-scale mechanisms, displacement efficiency, and precipitation phenomena by transmittance spectroscopy, fluorescence microscopy and thermal imaging (Figure 36).[193]

4.3.10. Microbial. Microbial improved and enhanced oil recovery (MIEOR) deploys microbes into wellbores and subsurface oil reservoirs and/or stimulates in-situ microbes to generate biochemicals that induce positive changes to reservoir and/or fluid conditions.[194] Although microbial has not been widely used in the oil industry, it is shown to be feasible in a number of laboratory experiments and field trials.[195] Armstrong et al. showed that microbial could produce a biosurfactant and bioclogging in water-wet micromodels. A pattern of 3D glass bead was photoetched into a silicon wafer, in which a series of solutions ranging from metabolically active bacteria to nutrient limited bacteria to dead inactive biomass were injected to assess the effectiveness of the proposed MEOR mechanisms.[196] Abolhasanzadeh et al. studied microbial EOR in oil-wet fractured micromodels. They used CO_2 laser engraving to fabricate plexiglass micromodels and compared water injection, surfactant injection, and microbial

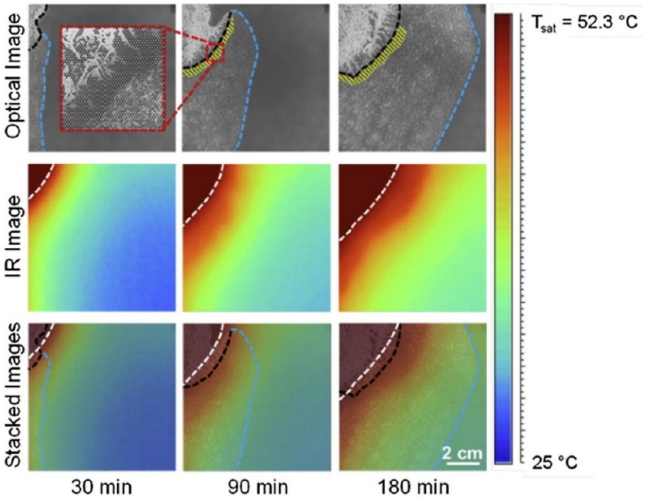

Figure 36. Optical, IR-thermal and stacked time-lapsed images of propane. Adapted with permission from ref 193. Copyright 2017 Elsevier.

injection in the micromodel, suggesting that the injection of bacterial enhanced the mobility ratio, decreased the brine/oil IFT, and altered the wettability of porous medium.[197] The wettability alteration is also investigated by Khajepour et al. They used bacterial that can produce biosurfactant and injected it into transparent glass micromodels. The relative permeability of micromodel after microbial treatment is also measured to show wettability alteration.[198] Gaol et al. analyzed the relation of microbial growth and transport in a silicon micromodel fabricated by lithography. They proposed that oil displacement of microbial was governed by microbial growth, bacteria community, properties of porous media and others (Figure 37).[199] Wang et al. studied the synergistic effect between microbial and surfactants on oil recovery in a 2D glass micromodel which had a similar pore structure with a natural sandstone. They suggested that synergistic effects on microbial metabolism and oil emulsification were the main contribution to oil recovery.[200]

4.4. Unconventional Reservoirs. Unconventional reservoirs have become an important portion of fossil hydrogen energy supplies as horizontal well and multistage hydraulic fracturing technology has advanced.[109,201] For most liquids in conventional reservoirs, the heat and mass transfer phenomena at the micro-scale still follow the conventional laws of continua. However, if one dimension of a channel shrinks to less than 100 nm, a number of new and interesting effects

https://doi.org/10.1021/acs.energyfuels.2c01943
Energy Fuels 2022, 36, 9904−9931

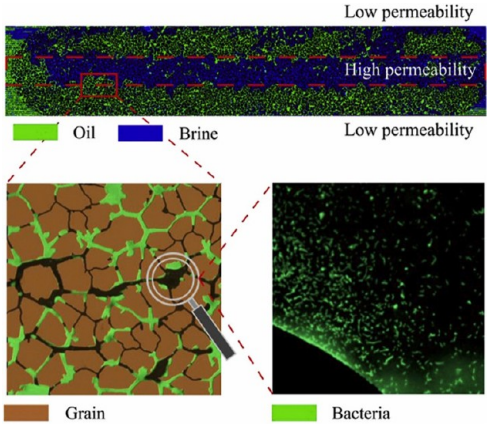

Figure 37. Oil, brine and bacteria in a micromodel. Reproduced with permission from ref 199. Copyright 2021 Elsevier.

emerge.[202] For example, Tas et al. found that water plugs in hydrophilic nanochannels could be significant negative pressure due to tensile capillary forces, resulting a curvature of the liquid meniscus (Figure 38).[203] Therefore, understanding oil recovery at the nano-scale requires the development of nanofluidic models in the last few decades.

Phase behaviors at the nano-scale can be observed in nanofluidic models. Plasma-etched microfluidic or nanofluidic models are known as the best candidate at unconventional scales because it can have a resolution in nanometers. Bao et al. fabricated a silicon-based nanochannel by deep dry etching. They studied hydrocarbon phase transition (liquid to vapor) in 88 nm channels in a pressure drawdown process. It was found that the cavitation pressure in the nanochannels corresponds closer to the spinodal limit than that predicted by the classical nucleation theory.[204] Zhong et al. quantified the methane/propane mixture phase behavior via direct imaging of connected channels from 10 nm to 10 μm with the supporting density functional theory.[205] In addition to a 1D nanochannel, Jatukaran et al. constructed 2D nanoporous media by using electron beam lithography on a silicon wafer. They also observed phase behaviors (evaporation) of oil/gas in a sub 10 nm scale and concluded that evaporation took place at pressures significantly lower than predictions from the Kelvin equation (Figure 39).[206] Ally et al. packed a bed of 150 nm diameter silica particles in a channel, and direct visualization of the fluid phase behavior was allowed by light scattering. They studied condensation of propane and carbon dioxide and showed that capillary condensation depends on pore geometry and wettability.[207] Yang et al. studied confinement effect on dew point pressure by combination of nanofluidics and molecular simulation. In the work, they visualized *n*-butane condensation in nanopores of 50, 10 and 4 nm. Both experimental results and molecular simulation showed that confinement effect had a significant impact on increasing the dew point pressure.[208]

Multiphase flow at the nano-scale can be studied in nanofluidic models. Wu et al. fabricated a 2D silicon nanofluidic model (channel depth is 100 nm) by dry etching. Using fluorescent signal correlation, they obtained and fitted flow rate and pressure drop in nanochannel into Poiseuille's Law.[209] They also visualized 1D gas−water and oil−water flow in the nanochannel with epi-fluorescence microscopy.[210,211] Combining both transport and phase change of nanoconfined fluid mixture, Zhong et al. developed a nanofluidic model with 2D nanoarrays and studied gas flooding and Huff-and-Puff strategies under miscible and immiscible conditions, by which they confirmed the applicability of the Lenormand phase diagram at nano-scale.[212] What is more, geomaterial based micromodel provides more realistically physicochemical properties. Porter et al. built a fracture matrix by etching on a thin shale section. They suggested that the shale micromodel exhibited more roughness due to the heterogeneous shale mineralogy, which had a significant effect on the multiphase flow process in the shale micromodel.[72]

Imbibition is the major oil recovery in a tight formation, which can be investigated by nanofluidic models. Kelly et al. first fabricated dual-scale micro/nanofluidic devices composed of a hydraulic fracture and a nano-scale matrix to mimic the low topological connectivity of nanoporous sedimentary rocks such as shale. The model is fabricated by a combination of transmission electron microscopy, dry etching, replica modeling with quartz, PDMS and polymer NOA 63 (Figure 40 left).[50] Kelly also investigated imbibition in silicon and glass nanochannels with various fluids, ketones, alcohols, aqueous solutions, and alkanes, at the nano-scale and they revealed that long-range intermolecular, electrostatic and solvation surface interactions played a significant role in nanocapillary imbibition. She also found a decreased capillary pressure in a decreased channel size, which is contradictory to the prediction of the Young−Laplace formula.[213] Zhang et al. used e-beam physical evaporation−deposition, a lift-off process and the anodic bonding method to fabricate a shale-like dual-porosity glass−silicon micro/nanofluidic model, which has a large width-to-depth ratio (12−2000). They found a fingering phenomenon with high viscosity of aqueous phase and the residual oil was dispersed in a variety of ways across the matrices, microfractures, and conduits. (Figure 40 right).[49] A micromodel can be used to analyze the recovery of fracturing fluid.[214] Hasham et al. visualized a fluid displacement during

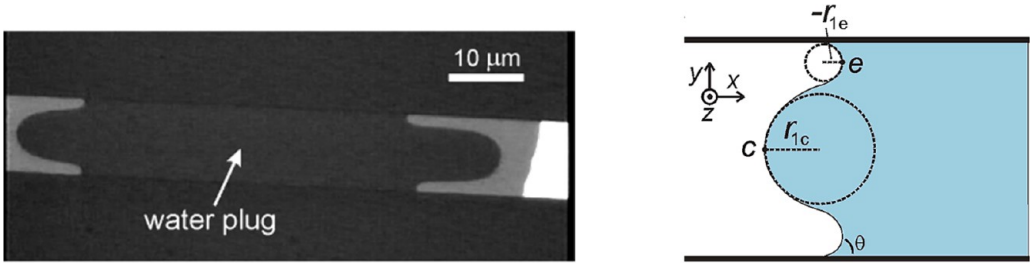

Figure 38. Optical micrograph of a water plug in a channel with 100 nm high (left). Top view of the meniscus curvature (right). Adapted with permission from ref 203. Copyright 2003 American Chemical Society.

https://doi.org/10.1021/acs.energyfuels.2c01943
Energy Fuels 2022, 36, 9904−9931

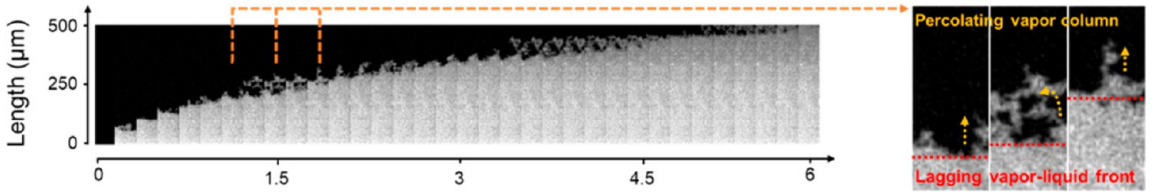

Figure 39. Evaporation at different times. The vapor phase appears bright and the liquid phase appears dark. Adapted with permission from ref 206. Copyright 2018 American Chemical Society.

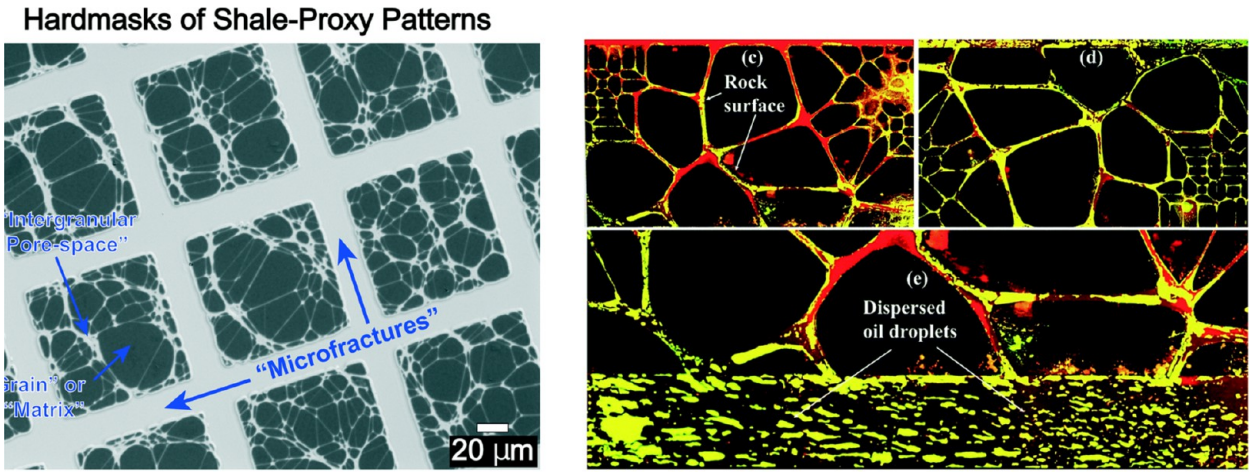

Figure 40. Image of a section of the synthetic shale network geometry after dry etching (left). Adapted with permission from ref 50. Copyright 2016 ROYAL SOCIETY OF CHEMISTRY. Residual oil distribution in the nanomatrix and microfractures (right). Reproduced with permission from ref 49. Copyright 2019 ROYAL SOCIETY OF CHEMISTRY.

hydraulic fracturing by using dry etched silicon−glass chips with circular and square grain shapes and identical depth of 175 nm.[215] Ayaz et al. conducted imbibition-drainage experiments in glass microfluidics and studied the two-phase fluid behavior in fracture-pore networks, revealing the extent of fracture fluid invasion.[216]

According to Table 4, 2D glass−silicon micromodels are the most applied in the oil and gas industry. The pore size and channel size are distributed from 4 nm to 1500 μm, in which nanofluidics to study phase behaviors of unconventional reservoir has the smallest pore size.

5. CHALLENGES AND OUTLOOK

Based on the review, a large number of microfluidics and nanofluidics have been applied widely in the oil and gas industry, providing merits in visualization, efficiency and low cost. However, there are many challenges limiting the further application of micromodels.

(1) Fabrication of 3D micro/nanomodels is still limited. The common methods to build 3D micromodels are replica molding,[10] 3D printing[11,225] and packing particles.[12] However, these methods have low resolutions, which limits the applications in small pore structure.[39] Besides, 3D printing lacks optically transparent, robust and pintable materials.[9]

(2) Pore/channel representability is not well designed. The surface roughness of the micromodel is still hard to be controlled. Although surface roughness does not influence flow behaviors in Darcy flow,[61] it has a significant effect on the multiphase flow process in the nanofluidic models.[72] Furthermore, many micromodels fail to account for the physicochemical features of real porous media, such as mineralogical composition and grain texture.

(3) Imaging techniques, including measuring and analyzing, needs to be improved. During fluid flow process, a large amount of imaging data at different stages needs to be analyzed, which is tremendously time-consuming.[9] Moreover, there is still difficulty of developing methods to characterize the contact angle and particle movement accounting for pore size, pore roughness, fluid-rock mineralogy at in-situ conditions.[6]

(4) Upscaling of fluid flow behaviors from micro/nanomodels to reservoir rocks is still challenging.[5] Fluid flow in the reservoir occurs from the nanometer to kilometer scale. Although there are many studies regarding combination of micromodel and numerical simulation, it is impossible to upscale their model solely to reservoirs because micromodel experiments usually have the limited spatial and time scale.

According to the review, we believe that the following research directions should be focused and developed in the future.

(1) Development of 3D micro/nanomodels that have realistic mineralogical composition, wettability, high resolution and better-controlled surface roughness.[71] It is worth to focus on improvement in 3D printing techniques and new materials that are low-cost, optically transparent, robust and pintable. Manufacturing of pores and channels in nanometer size is of great importance in the future because unconventional reservoirs will play more important roles.

(2) Advanced imaging techniques and microscopies should be introduced to micro/nanofluidics, including applica-

https://doi.org/10.1021/acs.energyfuels.2c01943
Energy Fuels 2022, 36, 9904−9931

Table 4. Summary of Micromodel Application in Oil and Gas Industry

Fields	Directions	Models	Pore/channel size	References
Fluid characterization	PVT analysis	1D glass-silicon microchannel, 2D glass-silicon microwells	15−200 μm	81−85
	Solubility and diffusivity	1D glass microchannel, 1D glass-silicon microchannel, 1D PMMA microchannel, 2D quartz particle packed model 2D silicon porous media	20−114 μm	86−95
Multiphase flow	Flow pattern and capillary number	2D silicon porous media, 2D glass porous media, 2D PDMS porous media, 2D Hele−Shaw cell, 2D NOA81 porous media, 3D glass-beads packed model	1.5−250 μm	1, 52, 73, 101−103
	Wettability	2D silicon porous media, 2D glass porous media, 2D PDMS porous media, 2D NOA81 porous media	1.5−900 μm	1, 101, 104−106
	Trapping phase	2D glass porous media, 2D silicon porous media 2D PDMS porous media	1.5−400 μm	1, 4, 22, 107−111
	Three-phase flow	2D PMMA cross-junction, 2D glass porous media, 2D silicon porous media, thin shale section	54−300 μm	2, 72, 112, 113
	Numerical simulation	2D glass porous media, 2D silicon porous media	1−940 μm	115−121
Enhanced oil recovery	Low-salinity water	1 D glass channel coated with $CaCO_3$, 2D glass porous media, 2D glass-beads packed model, 2D silicon porous media coated with kaolinite, thin sandstone section, 2D PDMS porous media	30−1500 μm	123−129, 217
	Polymer flooding	T-junction model 2D silicon porous media, 2D glass porous media 2D PDMS porous media	2−217 μm	132−137
	Surfactant	2D glass porous media, 2.5D glass porous media, T-junction model	5−200 μm	138, 140−144, 218
	Alkaline	2D glass porous media, 2D glass porous media	50−350 μm	145−148, 186−188, 190, 219
	Nanoparticle	2D silicon porous media, 2D glass porous media	6.4−450 μm	3, 151−155, 220
	In-situ gel	1D glass channel, 2D glass porous media	60−250 μm	157−160
	Preformed particle gel, including micro/nanogel	1D glass channel, 2D glass porous media, 3D glass-beads packed model	5−1500 μm	PPG: 162, 164−166, 221 Micro/nanogel: 168−172, 174−176
	Foam	2D silicon porous media, 2D glass porous media	13−250 μm	63, 178−185, 222, 223
	SAGD	2D glass porous media	56−118 μm	189, 190
	Solvent aided method	1D silicon channel, 2D PDMS porous media, 2D glass porous media	56−100 μm	191−193
	Microbial	2D silicon porous media, 2D glass porous media	10−286 μm	196, 198−200
Unconventional reservoir	Phase behaviors	1D silicon channel, 2D silicon porous media, 3D silica particle packed model	4−88 nm	204−208, 224
	Multiphase flow	1D silicon channel, 2D silicon porous media, thin shale section	50−277 nm, channel in shale section is 250 μm	49, 72, 209, 210
	Imbibition	2D polymer porous media, 2D silicon porous media	30−10000 nm	50, 71, 213, 215

tion of appropriate algorithm based on image analysis which offer accurate characterization of porous media and effective processing speed of fluid flow data in real time.[5,225,226] 4D CT techniques are gaining significant attention in the imaging industry.[12]

(3) There is a need to develop an integrated suite of tools that find averaged properties at different scales, which can be properly incorporated into simulations of relevant flow and transport processes at larger scales.[227]

(4) Machine learning and micro/nanofluidics will be combined in the modeling work of oil and gas fields since intelligent microfluidics, the convergence of machine learning and microfluidics, have been applied in materials science, medicine, and biotechnology in recent years.[228−231] Similarly, machine learning will also benefit microfluidics in petroleum engineering by autonomous interpretation of raw data, detection of complicated physicochemical phenomenon, and prediction of complex fluid flow with high accuracy.[232]

6. SUMMARY

This study reviews the fabrication methods, materials and applications of micro/nanofluidics in the oil and gas industry. From fabrication methods to micro/nanofluidic materials, we review the nonadditive manufacturing, additive manufacturing and packing particles methods. When it comes to applications in the oil and gas industry, a comprehensive review and summary is completed regarding fluid characterization, multiphase flow, various EOR methods and unconventional reservoirs. It shows that micro/nanofluidics have been widely employed because they can detect fluid flow characteristics and can be used as a modeling tool to disclose diverse oil recovery mechanisms. Finally, we propose the current challenges and future research directions based on the review. Development of novel 3D micro/nanomodels, imaging techniques, upscaling and machine learning methods are required to improve microfluidics and nanofluidics in the future.

AUTHOR INFORMATION

Corresponding Author

Baojun Bai − *Department of Geosciences and Geological and Petroleum Engineering, Missouri University of Science and Technology, Rolla, Missouri 65409, United States;* orcid.org/0000-0002-3551-4787; Email: baib@mst.edu

Authors

Junchen Liu − *Department of Geosciences and Geological and Petroleum Engineering, Missouri University of Science and Technology, Rolla, Missouri 65409, United States;* orcid.org/0000-0001-8300-0361

Yandong Zhang − *Department of Energy and Resources Engineering, Peking University, Beijing 10000, China*

https://doi.org/10.1021/acs.energyfuels.2c01943
Energy Fuels 2022, 36, 9904−9931

Mingzhen Wei − *Department of Geosciences and Geological and Petroleum Engineering, Missouri University of Science and Technology, Rolla, Missouri 65409, United States*
Xiaoming He − *Department of Mathematics and Statistics, Missouri University of Science and Technology, Rolla, Missouri 65409, United States*

Complete contact information is available at: https://pubs.acs.org/10.1021/acs.energyfuels.2c01943

Notes

The authors declare no competing financial interest.

Biographies

Junchen Liu is a Ph.D. candidate in Petroleum Engineering from Missouri University of Science and Technology. His research interests include polymer micro/nanogel transport in porous media and their EOR mechanisms.

Yandong Zhang is a postdoctoral researcher in Peking University. Dr. Zhang received his Ph.D. degree in Petroleum Engineering from Missouri University of Science and Technology. He focuses on multiphase flow in porous media at micro/nanoscopic level, development of micro/nanofluidics and CO_2 EOR methods.

Mingzhen Wei is an associate professor in Petroleum Engineering at the Department of GGPE in the Missouri University of Science and Technology. Dr. Wei received her Ph.D. degree in Computer Science from New Mexico Institute of Mining and Technology. Her research interests include data mining and data quality enhancement, application development to support digital oilfield initiations, and reservoir engineering and reservoir simulation for unconventional oil and gas development.

Xiaoming He is a professor in Department of Mathematics and Statistics at Missouri University of Science and Technology. Dr. He received his Ph.D. degree in Mathematics at Virginia Polytechnic Institute and State University. His research interests include interface problems, multiphase problems, computational fluid, data assimilation, stochastic PDEs, boundary integral equations, feedback control, finite element methods, domain decomposition methods, lattice Boltzmann methods, extrapolations and computational plasma physics (Particle-In-Cell method).

Baojun Bai is a professor in Petroleum Engineering at the Department of GGPE in the Missouri University of Science and Technology. Dr. Bai received his Ph.D. degree in Petroleum Engineering from New Mexico Institute of Mining and Technology. His research interests include conformance control, chemical EOR methods, CCUS, reservoir numerical simulation and multiphase flow in porous media.

■ ACKNOWLEDGMENTS

The authors would like to acknowledge National Science Foundation for funding through grants DMS-1722647 and DMS-2152609.

■ REFERENCES

(1) Yun, W.; Ross, C. M.; Roman, S.; Kovscek, A. R. Creation of a Dual-Porosity and Dual-Depth Micromodel for the Study of Multiphase Flow in Complex Porous Media. *Lab Chip* **2017**, *17* (8), 1462−1474.
(2) Yue, J.; Rebrov, E. V.; Schouten, J. C. Gas-Liquid-Liquid Three-Phase Flow Pattern and Pressure Drop in a Microfluidic Chip: Similarities with Gas-Liquid/Liquid-Liquid Flows. *Lab Chip* **2014**, *14* (9), 1632−1649.
(3) Suzuki, A.; Cui, J.; Zhang, Y.; Uehara, S.; Li, K.; Horne, R. N.; Ito, T. Experimental Study on Nano-/Microparticles Transport to Characterize Structures in Fractured Porous Media. *Rock Mech. Rock Eng.* **2020**, *53* (10), 4357−4365.
(4) Haque, N.; Singh, A.; Saha, U. K. Experimental Visualization and Analysis of Multiphase Immiscible Flow in Fractured Micromodels Using Micro-Particle Image Velocimetry. *J. Energy Resour. Technol. Trans. ASME* **2022**, *144* (2). DOI: 10.1115/1.4050958.
(5) Gaol, C. L.; Wegner, J.; Ganzer, L. Real Structure Micromodels Based on Reservoir Rocks for Enhanced Oil Recovery (EOR) Applications. *Lab Chip* **2020**, *20* (12), 2197−2208.
(6) Fani, M.; Pourafshary, P.; Mostaghimi, P.; Mosavat, N. Application of Microfluidics in Chemical Enhanced Oil Recovery: A Review. *Fuel* **2022**, *315* (July 2021), 123225.
(7) Gogoi, S.; Gogoi, S. B. Review on Microfluidic Studies for EOR Application. *J. Pet. Explor. Prod. Technol.* **2019**, *9* (3), 2263−2277.
(8) Karadimitriou, N. K.; Hassanizadeh, S. M. A Review of Micromodels and Their Use in Two-Phase Flow Studies. *Vadose Zo. J.* **2012**, *11* (3), vzj2011.0072.
(9) Cao, S. C.; Jung, J.; Radonjic, M. Application of Microfluidic Pore Models for Flow, Transport, and Reaction in Geological Porous Media: From a Single Test Bed to Multifunction Real-Time Analysis Tool. *Microsyst. Technol.* **2019**, *25* (11), 4035−4052.
(10) Anbari, A.; Chien, H. T.; Datta, S. S.; Deng, W.; Weitz, D. A.; Fan, J. Microfluidic Model Porous Media: Fabrication and Applications. *Small* **2018**, *14* (18), 1703575.
(11) Lifton, V. A. Microfluidics: An Enabling Screening Technology for Enhanced Oil Recovery (EOR). *Lab Chip* **2016**, *16* (10), 1777−1796.
(12) Jahanbakhsh, A.; Wlodarczyk, K. L.; Hand, D. P.; Maier, R. R. J.; Maroto-Valer, M. M. Review of Microfluidic Devices and Imaging Techniques for Fluid Flow Study in Porous Geomaterials. *Sensors (Switzerland).* **2020**, *20* (14), 4030.
(13) Deng, T.; Wu, H.; Brittain, S. T.; Whitesides, G. M. Prototyping of Masks, Masters, and Stamps/Molds for Soft Lithography Using an Office Printer and Photographic Reduction. *Anal. Chem.* **2000**, *72* (14), 3176−3180.
(14) Nguyen, H. T.; Thach, H.; Roy, E.; Huynh, K.; Perrault, C. M. T. Low-Cost, Accessible Fabrication Methods for Microfluidics Research in Low-Resource Settings. *Micromachines* **2018**, *9*, 461.
(15) Revzin, A.; Russell, R. J.; Yadavalli, V. K.; Koh, W. G.; Deister, C.; Hile, D. D.; Mellott, M. B.; Pishko, M. V. Fabrication of Poly(Ethylene Glycol) Hydrogel Microstructures Using Photolithography. *Langmuir.* **2001**, *17*, 5440−5447.
(16) Xia, Y.; Whitesides, G. M. Soft Lithography. *Angew. Chemie Int. Ed.* **1998**, *37* (5), 550−575.
(17) Raj M, K.; Chakraborty, S. PDMS Microfluidics: A Mini Review. *J. Appl. Polym. Sci.* **2020**, *137* (27), 48958.
(18) McDonald, J. C.; Duffy, D. C.; Anderson, J. R.; Chiu, D. T.; Wu, H.; Schueller, O. J. A.; Whitesides, G. M. Fabrication of Microfluidic Systems in PDMS. *Electrophoresis* **2000**, *21* (1), 27−40.
(19) Bien, D. C. S.; Rainey, P. V.; Mitchell, S. J. N.; Gamble, H. S. Characterization of Masking Materials for Deep Glass Micromachining. *J. Micromechanics Microeng.* **2003**, *13* (4), S34.
(20) Iliescu, C.; Chen, B.; Miao, J. On the Wet Etching of Pyrex Glass. *Sensors Actuators, A Phys.* **2008**, *143* (1), 154−161.
(21) Iliescu, C.; Tay, F. E. H. Wet Etching of Glass. *Proceedings of the International Semiconductor Conference, CAS*; IEEE: New York, 2005; Vol. *1*, pp 35−44..
(22) Xu, K.; Liang, T.; Zhu, P.; Qi, P.; Lu, J.; Huh, C.; Balhoff, M. A 2.5-D Glass Micromodel for Investigation of Multi-Phase Flow in Porous Media. *Lab Chip* **2017**, *17* (4), 640−646.
(23) Racka-Szmidt, K.; Stonio, B.; Żelazko, J.; Filipiak, M.; Sochacki, M. A Review: Inductively Coupled Plasma Reactive Ion Etching of Silicon Carbide. *Materials (Basel)* **2022**, *15* (1), 123.
(24) He, B.; Yang, Y.; Yuen, M. F.; Chen, X. F.; Lee, C. S.; Zhang, W. J. Vertical Nanostructure Arrays by Plasma Etching for Applications in Biology, Energy, and Electronics. *Nano Today* **2013**, *8* (3), 265−289.

(25) Wang, S.; Zhou, Z.; Li, B.; Wang, C.; Liu, Q. Progresses on New Generation Laser Direct Writing Technique. *Mater. Today Nano* **2021**, *16*, 100142.
(26) Gittard, S. D.; Narayan, R. J. Laser Direct Writing of Micro- and Nano-Scale Medical Devices. *Expert Rev. Med. Devices* **2010**, *7* (3), 343−356.
(27) Wlodarczyk, K. L.; Hand, D. P.; Maroto-Valer, M. M. Maskless, Rapid Manufacturing of Glass Microfluidic Devices Using a Picosecond Pulsed Laser. *Sci. Rep.* **2019**, *9* (1), 1−13.
(28) Scott, S. M.; Ali, Z. Fabrication Methods for Microfluidic Devices: An Overview. *Micromachines.* **2021**, *12*, 319.
(29) Mishra, S.; Yadava, V. Laser Beam MicroMachining (LBMM) - A Review. *Opt. Lasers Eng.* **2015**, *73*, 89−122.
(30) Doryani, H.; Malayeri, M. R.; Riazi, M. Visualization of Asphaltene Precipitation and Deposition in a Uniformly Patterned Glass Micromodel. *Fuel* **2016**, *182*, 613−622.
(31) Desbiens, J. P.; Masson, P. ArF Excimer Laser Micromachining of Pyrex, SiC and PZT for Rapid Prototyping of MEMS Components. *Sensors Actuators, A Phys.* **2007**, *136* (2), 554−563.
(32) Mohajeri, M.; Hemmati, M.; Shekarabi, A. S. An Experimental Study on Using a Nanosurfactant in an EOR Process of Heavy Oil in a Fractured Micromodel. *J. Pet. Sci. Eng.* **2015**, *126*, 162−173.
(33) Deshmukh, S. S.; Goswami, A. Hot Embossing of Polymers - A Review. *Mater. Today Proc.* **2020**, *26* (xxxx), 405−414.
(34) Becker, H.; Heim, U. Hot Embossing as a Method for the Fabrication of Polymer High Aspect Ratio Structures. *Sensors Actuators, A Phys.* **2000**, *83* (1), 130−135.
(35) Yeo, L. P.; Ng, S. H.; Wang, Z. F.; Xia, H. M.; Wang, Z. P.; Thang, V. S.; Zhong, Z. W.; De Rooij, N. F. Investigation of Hot Roller Embossing for Microfluidic Devices. *J. Micromechanics Microeng.* **2010**, *20* (1), 015017.
(36) Sequeiros, E. W.; Emadinia, O.; Vieira, M. T.; Vieira, M. F. Development of Metal Powder Hot Embossing: A New Method for Micromanufacturing. *Metals (Basel)* **2020**, *10* (3), 388.
(37) Nielsen, J. B.; Hanson, R. L.; Almughamsi, H. M.; Pang, C.; Fish, T. R.; Woolley, A. T. Microfluidics: Innovations in Materials and Their Fabrication and Functionalization. *Anal. Chem.* **2020**, *92* (1), 150−168.
(38) Bhattacharjee, N.; Urrios, A.; Kang, S.; Folch, A. The Upcoming 3D-Printing Revolution in Microfluidics. *Lab Chip* **2016**, *16* (10), 1720−1742.
(39) He, Y.; Wu, Y.; Fu, J. Z.; Gao, Q.; Qiu, J. J. Developments of 3D Printing Microfluidics and Applications in Chemistry and Biology: A Review. *Electroanalysis* **2016**, *28* (8), 1658−1678.
(40) Rupal, B. S.; Garcia, E. A.; Ayranci, C.; Qureshi, A. J. 3D Printed 3D-Microfluidics: Recent Developments and Design Challenges. *J. Integr. Des. Process Sci.* **2019**, *22* (1), 5−20.
(41) Bressan, L. P.; Adamo, C. B.; Quero, R. F.; De Jesus, D. P.; Da Silva, J. A. F. A Simple Procedure to Produce FDM-Based 3D-Printed Microfluidic Devices with an Integrated PMMA Optical Window. *Anal. Methods* **2019**, *11* (8), 1014−1020.
(42) Lynh, H. D.; Pin-Chuan, C. Novel Solvent Bonding Method for Creation of a Three-Dimensional, Non-Planar, Hybrid PLA/PMMA Microfluidic Chip. *Sensors and Actuators, A: Physical.* **2018**, *280*, 350−358.
(43) Lifton, V. A.; Lifton, G.; Simon, S. Options for Additive Rapid Prototyping Methods (3D Printing) in MEMS Technology. *Rapid Prototyp. J.* **2014**, *20* (5), 403−412.
(44) Kruth, J.-P.; Wang, X.; Laoui, T.; Froyen, L. Lasers and Materials in Selective Laser Sintering. *Assem. Autom.* **2003**, *23*, 357−371.
(45) Au, A. K.; Huynh, W.; Horowitz, L. F.; Folch, A. 3D-Printed Microfluidics. *Angew. Chemie - Int. Ed.* **2016**, *55* (12), 3862−3881.
(46) Nagarajan, B.; Hu, Z.; Song, X.; Zhai, W.; Wei, J. Development of Micro Selective Laser Melting: The State of the Art and Future Perspectives. *Engineering* **2019**, *5* (4), 702−720.
(47) Yan, B.; Liu, S.; Heng, Y. Nano-Oxide Thin Films Deposited via Atomic Layer Deposition on Microchannel Plates. *Nanoscale Res. Lett.* **2015**, *10* (1), 1−11.
(48) Chen, X.; Zhang, L. Review in Manufacturing Methods of Nanochannels of Bio-Nanofluidic Chips. *Sensors Actuators, B Chem.* **2018**, *254*, 648−659.
(49) Zhang, Y.; Zhou, C.; Qu, C.; Wei, M.; He, X.; Bai, B. Fabrication and Verification of a Glass-Silicon-Glass Micro-/Nano-fluidic Model for Investigating Multi-Phase Flow in Shale-like Unconventional Dual-Porosity Tight Porous Media. *Lab Chip* **2019**, *19* (24), 4071−4082.
(50) Kelly, S. A.; Torres-Verdín, C.; Balhoff, M. T. Subsurface to Substrate: Dual-Scale Micro/Nanofluidic Networks for Investigating Transport Anomalies in Tight Porous Media. *Lab Chip* **2016**, *16* (15), 2829−2839.
(51) Zhang, Y.; Khorshidian, H.; Mohammadi, M.; Sanati-Nezhad, A.; Hejazi, S. H. Functionalized Multiscale Visual Models to Unravel Flow and Transport Physics in Porous Structures. *Water Res.* **2020**, *175*, 115676.
(52) Krummel, A. T.; Datta, S. S.; Münster, S.; Weitz, D. A. Visualizing Multiphase Flow and Trapped Fluid Configurations in a Model Three-dimensional Porous Medium. *AIChE J.* **2013**, *59* (3), 1022−1029.
(53) Oosterbroek, R. E.; Hermes, D. C.; Kakuta, M.; Benito-Lopez, F.; Gardeniers, J. G. E.; Verboom, W.; Reinhoudt, D. N.; Van Den Berg, A. Fabrication and Mechanical Testing of Glass Chips for High-Pressure Synthetic or Analytical Chemistry. *Microsyst. Technol.* **2006**, *12* (5), 450−454.
(54) Tiggelaar, R. M.; Benito-López, F.; Hermes, D. C.; Rathgen, H.; Egberink, R. J. M.; Mugele, F. G.; Reinhoudt, D. N.; van den Berg, A.; Verboom, W.; Gardeniers, H. J. G. E. Fabrication, Mechanical Testing and Application of High-Pressure Glass Microreactor Chips. *Chem. Eng. J.* **2007**, *131* (1−3), 163−170.
(55) Wang, W.; Chang, S.; Gizzatov, A. Toward Reservoir-on-a-Chip: Fabricating Reservoir Micromodels by in Situ Growing Calcium Carbonate Nanocrystals in Microfluidic Channels. *ACS Appl. Mater. Interfaces* **2017**, *9* (34), 29380−29386.
(56) Gerami, A.; Alzahid, Y.; Mostaghimi, P.; Kashaninejad, N.; Kazemifar, F.; Amirian, T.; Mosavat, N.; Ebrahimi Warkiani, M.; Armstrong, R. T. Microfluidics for Porous Systems: Fabrication, Microscopy and Applications. *Transp. Porous Media* **2019**, *130* (1), 277−304.
(57) Sivakumar, R.; Lee, N. Y. Microfluidic Device Fabrication Mediated by Surface Chemical Bonding. *Analyst* **2020**, *145* (12), 4096−4110.
(58) Allen, P. B.; Chiu, D. T. Calcium-Assisted Glass-to-Glass Bonding for Fabrication of Glass Microfluidic Devices. *Anal. Chem.* **2008**, *80* (18), 7153−7157.
(59) Chen, L.; Luo, G.; Liu, K.; Ma, J.; Yao, B.; Yan, Y.; Wang, Y. Bonding of Glass-Based Microfluidic Chips at Low- or Room-Temperature in Routine Laboratory. *Sensors Actuators, B Chem.* **2006**, *119* (1), 335−344.
(60) Lima, R. S.; Leão, P. A. G. C.; Piazzetta, M. H. O.; Monteiro, A. M.; Shiroma, L. Y.; Gobbi, A. L.; Carrilho, E. Sacrificial Adhesive Bonding: A Powerful Method for Fabrication of Glass Microchips. *Sci. Rep.* **2015**, *5*, 1−15.
(61) Gjengedal, S.; Brøtan, V.; Buset, O. T.; Larsen, E.; Berg, O.; Torsæter, O.; Ramstad, R. K.; Hilmo, B. O.; Frengstad, B. S. Fluid Flow through 3D-Printed Particle Beds: A New Technique for Understanding, Validating, and Improving Predictability of Permeability from Empirical Equations. *Transport Porous Media* **2020**, *134*, 1−40.
(62) Morais, S.; Cario, A.; Liu, N.; Bernard, D.; Lecoutre, C.; Garrabos, Y.; Ranchou-Peyruse, A.; Dupraz, S.; Azaroual, M.; Hartman, R. L.; Marre, S. Studying Key Processes Related to CO2underground Storage at the Pore Scale Using High Pressure Micromodels. *React. Chem. Eng.* **2020**, *5* (7), 1156−1185.
(63) Almajid, M. M.; Kovscek, A. R. Pore-Level Mechanics of Foam Generation and Coalescence in the Presence of Oil. *Adv. Colloid Interface Sci.* **2016**, *233*, 65−82.
(64) Johnston, I. D.; McCluskey, D. K.; Tan, C. K. L.; Tracey, M. C. Mechanical Characterization of Bulk Sylgard 184 for Microfluidics

https://doi.org/10.1021/acs.energyfuels.2c01943
Energy Fuels 2022, 36, 9904−9931

and Microengineering. *J. Micromechanics Microeng.* **2014**, *24* (3), 035017.
(65) Guzmán-Meza, M.; Laurindo, J. B.; Jarpa-Parra, M.; Segura-Ponce, L. Isothermal Drying of Plant-Based Food Material: An Approach Using 2D Polydimethylsiloxane (PDMS) Micromodels. *Chem. Eng. Sci.* **2020**, *215*, 115385.
(66) Sun, Y. S. Studying Electrotaxis in Microfluidic Devices. *Sensors (Switzerland).* **2017**, *17*, 2048.
(67) Nguyen, T.; Jung, S. H.; Lee, M. S.; Park, T. E.; Ahn, S. K.; Kang, J. H. Robust Chemical Bonding of PMMA Microfluidic Devices to Porous PETE Membranes for Reliable Cytotoxicity Testing of Drugs. *Lab Chip* **2019**, *19* (21), 3706−3713.
(68) Song, W.; De Haas, T. W.; Fadaei, H.; Sinton, D. Chip-off-the-Old-Rock: The Study of Reservoir-Relevant Geological Processes with Real-Rock Micromodels. *Lab Chip* **2014**, *14* (22), 4382−4390.
(69) Bowden, S. A.; Tanino, Y.; Akamairo, B.; Christensen, M. Recreating Mineralogical Petrographic Heterogeneity within Microfluidic Chips: Assembly, Examples, and Applications. *Lab Chip* **2016**, *16* (24), 4677−4681.
(70) Zhang, Y. Q.; Sanati-Nezhad, A.; Hejazi, S. H. Geo-Material Surface Modification of Microchips Using Layer-by-Layer (LbL) Assembly for Subsurface Energy and Environmental Applications. *Lab Chip* **2018**, *18* (2), 285−295.
(71) Mehmani, A.; Kelly, S.; Torres-Verdín, C. Micro/Nanofluidic Insights on Fluid Deliverability Controls in Tight Rocks. *SPWLA 60th Annual Logging Symposium*, The Woodlands, TX, June 15−19, 2019; OnePetro, 2019; SPWLA-2019-QQ..
(72) Porter, M. L.; Jiménez-Martínez, J.; Martinez, R.; McCulloch, Q.; Carey, J. W.; Viswanathan, H. S. Geo-Material Microfluidics at Reservoir Conditions for Subsurface Energy Resource Applications. *Lab Chip* **2015**, *15* (20), 4044−4053.
(73) Chatenever, A.; Calhoun, J. C. Visual Examinations of Fluid Behavior in Porous Media-Part I. *J. Pet. Technol.* **1952**, *4* (06), 149−156.
(74) Paterson, L.; Hornof, V.; Neale, G. A Consolidated Porous Medium for the Visualization of Unstable Displacements. *Powder Technol.* **1982**, *33* (2), 265−268.
(75) Mattax, C. C.; Kyte, J. R. Ever See a Water Flood. *Oil Gas J.* **1961**, *59* (42), 115−128.
(76) Schwartz, G. C.; Schaible, P. M. Reactive Ion Etching of Silicon. *J. Vac. Sci. Technol.* **1979**, *16* (2), 410−413.
(77) Danesh, A.; Peden, J. M.; Krinis, D.; Henderson, G. D. Pore Level Visual Investigation of Oil Recovery by Solution Gas Drive and Gas Injection. In *Proceedings of the SPE Annual Technical Conference and Exhibition*, Dallas, TX, September 27, 1987; OnePetro, 1987; SPE-16956-MS.
(78) Stoner, D. L.; Watson, S. M.; Stedtfeld, R. D.; Meakin, P.; Griffel, L. K.; Tyler, T. L.; Pegram, L. M.; Barnes, J. M.; Deason, V. A. Application of Stereolithographic Custom Models for Studying the Impact of Biofilms and Mineral Precipitation on Fluid Flow. *Appl. Environ. Microbiol.* **2005**, *71* (12), 8721−8728.
(79) Maghzi, A.; Mohammadi, S.; Ghazanfari, M. H.; Kharrat, R.; Masihi, M. Monitoring Wettability Alteration by Silica Nanoparticles during Water Flooding to Heavy Oils in Five-Spot Systems: A Pore-Level Investigation. *Exp. Therm. Fluid Sci.* **2012**, *40*, 168−176.
(80) Gavoille, T.; Pannacci, N.; Bergeot, G.; Marliere, C.; Marre, S. Microfluidic Approaches for Accessing Thermophysical Properties of Fluid Systems. *React. Chem. Eng.* **2019**, *4* (10), 1721−1739.
(81) Mostowfi, F.; Molla, S.; Tabeling, P. Determining Phase Diagrams of Gas-Liquid Systems Using a Microfluidic PVT. *Lab Chip* **2012**, *12* (21), 4381−4387.
(82) Molla, S.; Mostowfi, F. Microfluidic Platform for PVT Measurements. In *Proceedings of the SPE Annual Technical Conference and Exhibition*, Amsterdam, The Netherlands, October 27−29, 2014; OnePetro, 2014; SPE-170910-MS.
(83) Pinho, B.; Girardon, S.; Bazer-Bachi, F.; Bergeot, G.; Marre, S.; Aymonier, C. A Microfluidic Approach for Investigating Multicomponent System Thermodynamics at High Pressures and Temperatures. *Lab Chip* **2014**, *14* (19), 3843−3849.
(84) Bao, B.; Riordon, J.; Xu, Y.; Li, H.; Sinton, D. Direct Measurement of the Fluid Phase Diagram. *Anal. Chem.* **2016**, *88* (14), 6986−6989.
(85) Xu, Y.; Riordon, J.; Cheng, X.; Bao, B.; Sinton, D. The Full Pressure-Temperature Phase Envelope of a Mixture in 1000 Microfluidic Chambers. *Angew. Chem.* **2017**, *129* (45), 14150−14155.
(86) Fisher, R.; Shah, M. K.; Eskin, D.; Schmidt, K.; Singh, A.; Molla, S.; Mostowfi, F. Equilibrium Gas-Oil Ratio Measurements Using a Microfluidic Technique. *Lab Chip* **2013**, *13* (13), 2623−2633.
(87) Molla, S.; Mostowfi, F. Microfluidic PVT-Saturation Pressure and Phase-Volume Measurement of Black Oils. *SPE Reserv. Eval. Eng.* **2017**, *20* (1), 233−239.
(88) Molla, S.; Magro, L.; Mostowfi, F. Microfluidic Technique for Measuring Wax Appearance Temperature of Reservoir Fluids. *Lab Chip* **2016**, *16* (19), 3795−3803.
(89) Schneider, M. H.; Sieben, V. J.; Kharrat, A. M.; Mostowfi, F. Measurement of Asphaltenes Using Optical Spectroscopy on a Microfluidic Platform. *Anal. Chem.* **2013**, *85* (10), 5153−5160.
(90) Hu, C.; Morris, J. E.; Hartman, R. L. Microfluidic Investigation of the Deposition of Asphaltenes in Porous Media. *Lab Chip* **2014**, *14* (12), 2014−2022.
(91) Qi, Z.; Abedini, A.; Sharbatian, A.; Pang, Y.; Guerrero, A.; Sinton, D. Asphaltene Deposition during Bitumen Extraction with Natural Gas Condensate and Naphtha. *Energy Fuels* **2018**, *32* (2), 1433−1439.
(92) Fadaei, H.; Scarff, B.; Sinton, D. Rapid Microfluidics-Based Measurement of CO2 Diffusivity in Bitumen. *Energy Fuels* **2011**, *25* (10), 4829−4835.
(93) Sell, A.; Fadaei, H.; Kim, M.; Sinton, D. Measurement of CO2 Diffusivity for Carbon Sequestration: A Microfluidic Approach for Reservoir-Specific Analysis. *Environ. Sci. Technol.* **2013**, *47*, 71−78.
(94) Nguyen, P.; Mohaddes, D.; Riordon, J.; Fadaei, H.; Lele, P.; Sinton, D. Fast Fluorescence-Based Microfluidic Method for Measuring Minimum Miscibility Pressure of CO2 in Crude Oils. *Anal. Chem.* **2015**, *87* (6), 3160−3164.
(95) Sharbatian, A.; Abedini, A.; Qi, Z.; Sinton, D. Full Characterization of CO2-Oil Properties On-Chip: Solubility, Diffusivity, Extraction Pressure, Miscibility, and Contact Angle. *Anal. Chem.* **2018**, *90* (4), 2461−2467.
(96) Li, Y.; Ward, K. R.; Burns, M. A. Viscosity Measurements Using Microfluidic Droplet Length. *Anal. Chem.* **2017**, *89* (7), 3996−4006.
(97) Lan, W. J.; Li, S. W.; Xu, J. H.; Luo, G. S. Rapid Measurement of Fluid Viscosity Using Co-Flowing in a Co-Axial Microfluidic Device. *Microfluid. Nanofluidics* **2010**, *8* (5), 687−693.
(98) Guillot, P.; Panizza, P.; Salmon, J. B.; Joanicot, M.; Colin, A.; Bruneau, C. H.; Colin, T. Viscosimeter on a Microfluidic Chip. *Langmuir* **2006**, *22* (14), 6438−6445.
(99) Pinho, B.; Girardon, S.; Bazer-Bachi, F.; Bergeot, G.; Marre, S.; Aymonier, C. Simultaneous Measurement of Fluids Density and Viscosity Using HP/HT Capillary Devices. *J. Supercrit. Fluids* **2015**, *105*, 186−192.
(100) Cakmak, O.; Ermek, E.; Kilinc, N.; Yaralioglu, G. G.; Urey, H. Precision Density and Viscosity Measurement Using Two Cantilevers with Different Widths. *Sensors Actuators A Phys.* **2015**, *232*, 141−147.
(101) Zhao, B.; MacMinn, C. W.; Juanes, R. Wettability Control on Multiphase Flow in Patterned Microfluidics. *Proc. Natl. Acad. Sci. U. S. A.* **2016**, *113* (37), 10251−10256.
(102) Datta, S. S.; Dupin, J. B.; Weitz, D. A. Fluid Breakup during Simultaneous Two-Phase Flow through a Three-Dimensional Porous Medium. *Phys. Fluids* **2014**, *26* (6), 062004.
(103) Cottin, C.; Bodiguel, H.; Colin, A. Drainage in Two-Dimensional Porous Media: From Capillary Fingering to Viscous Flow. *Phys. Rev. E - Stat. Nonlinear, Soft Matter Phys.* **2010**, *82* (4), 1−10.
(104) Maaref, S.; Rokhforouz, M. R.; Ayatollahi, S. Numerical Investigation of Two Phase Flow in Micromodel Porous Media: Effects of Wettability, Heterogeneity, and Viscosity. *Can. J. Chem. Eng.* **2017**, *95* (6), 1213−1223.

https://doi.org/10.1021/acs.energyfuels.2c01943
Energy Fuels 2022, 36, 9904−9931

(105) Schneider, M. H.; Tabeling, P. Lab-on-Chip Methodology in the Energy Industry: Wettability Patterns and Their Impact on Fluid Displacement in Oil Reservoir Models. *Am. J. Appl. Sci.* **2011**, *8* (10), 927−932.
(106) Ma, K.; Rivera, J.; Hirasaki, G. J.; Biswal, S. L. Wettability Control and Patterning of PDMS Using UV-Ozone and Water Immersion. *J. Colloid Interface Sci.* **2011**, *363* (1), 371−378.
(107) Chatzis, I.; Morrow, N. R.; Lim, H. T. Magnitude and Detailed Structure of Residual Oil Saturation. *Soc. Pet. Eng. J.* **1983**, *23* (2), 311−326.
(108) Roman, S.; Soulaine, C.; AlSaud, M. A.; Kovscek, A.; Tchelepi, H. Particle Velocimetry Analysis of Immiscible Two-Phase Flow in Micromodels. *Adv. Water Resour.* **2016**, *95*, 199−211.
(109) Liang, X.; Zhou, F.; Liang, T.; Su, H.; Yuan, S.; Li, Y. Impacts of Pore Structure and Wettability on Distribution of Residual Fossil Hydrogen Energy after Imbibition. *Int. J. Hydrogen Energy* **2020**, *45* (29), 14779−14789.
(110) Rodríguez de Castro, A.; Oostrom, M.; Shokri, N. Effects of Shear-Thinning Fluids on Residual Oil Formation in Microfluidic Pore Networks. *J. Colloid Interface Sci.* **2016**, *472*, 34−43.
(111) Tian, J.; Kang, Y.; You, L.; Jia, N.; Xi, Z.; Luo, P. Investigation on Water Phase Trapping Mechanisms in Tight Gas Reservoirs: Pore-Scale Visualization Observation and Core-Scale Flooding Analysis. *J. Pet. Sci. Eng.* **2021**, *198* (October 2020), 108185.
(112) Wang, K.; Lu, Y.; Qin, K.; Luo, G.; Wang, T. Generating Gas-Liquid-Liquid Three-Phase Microflows in a Cross-Junction Microchannel Device. *Chem. Eng. Technol.* **2013**, *36* (6), 1047−1060.
(113) Lu, H.; Huang, F.; Jiang, P.; Xu, R. Exsolution Effects in CO2 Huff-n-Puff Enhanced Oil Recovery: Water-Oil-CO2 Three Phase Flow Visualization and Measurements by Micro-PIV in Micromodel. *Int. J. Greenh. Gas Control* **2021**, *111* (May), 103445.
(114) Golparvar, A.; Zhou, Y.; Wu, K.; Ma, J.; Yu, Z. A Comprehensive Review of Pore Scale Modeling Methodologies for Multiphase Flow in Porous Media. *Adv. Geo-Energy Res.* **2018**, *2* (4), 418−440.
(115) Liu, H.; Sun, S.; Wu, R.; Wei, B.; Hou, J. Pore-Scale Modeling of Spontaneous Imbibition in Porous Media Using the Lattice Boltzmann Method. *Water Resour. Res.* **2021**, *57* (6), 1−24.
(116) Tian, Y.; Ju, B.; Chen, X.; Chen, Z.; Dong, Y.; Wu, D. Pore-Scale Investigation of Waterflooding Based on Experiments and Numerical Simulations Considering the Change in Geometry and Wettability. *Energy Fuels* **2021**, *35* (21), 17617−17628.
(117) Bandara, U. C.; Tartakovsky, A. M.; Oostrom, M.; Palmer, B. J.; Grate, J.; Zhang, C. Smoothed Particle Hydrodynamics Pore-Scale Simulations of Unstable Immiscible Flow in Porous Media. *Adv. Water Resour.* **2013**, *62*, 356−369.
(118) Zhang, C.; Oostrom, M.; Wietsma, T. W.; Grate, J. W.; Warner, M. G. Influence of Viscous and Capillary Forces on Immiscible Fluid Displacement: Pore-Scale Experimental Study in a Water-Wet Micromodel Demonstrating Viscous and Capillary Fingering. *Energy Fuels* **2011**, *25* (8), 3493−3505.
(119) Jung, M.; Brinkmann, M.; Seemann, R.; Hiller, T.; Sanchez De La Lama, M.; Herminghaus, S. Wettability Controls Slow Immiscible Displacement through Local Interfacial Instabilities. *Phys. Rev. Fluids* **2016**, *1* (7), 1−19.
(120) Ferrari, A.; Jimenez-Martinez, J.; Le Borgne, T.; Méheust, Y.; Lunati, I. Challenges in Modeling Unstable Two-Phase Flow Experiments in Porous Micromodels. *Water Resources Res.* **2015**, *51*, 1381−1400.
(121) Niasar, V. J.; Hassanizadeh, S. M.; Pyrak-Nolte, L. J.; Berentsen, C. Simulating Drainage and Imbibition Experiments in a High-Porosity Micromodel Using an Unstructured Pore Network Model. *Water Resourses Res.* **2009**, *45* (2), 1−15.
(122) Bartels, W. B.; Mahani, H.; Berg, S.; Hassanizadeh, S. M. Literature Review of Low Salinity Waterflooding from a Length and Time Scale Perspective. *Fuel* **2019**, *236* (September 2018), 338−353.
(123) Shaik, I. K.; Aichele, C. P.; Bikkina, P. K. Microfluidics-Based Low Salinity Wettability Alteration Study of Naphthenic-Acid-Adsorbed Calcite Surfaces. *Energy Fuels* **2022**, *36* (4), 1842−1853.
(124) Bartels, W. B.; Mahani, H.; Berg, S.; Menezes, R.; Van Der Hoeven, J. A.; Fadili, A. Oil Configuration under High-Salinity and Low-Salinity Conditions at Pore Scale: A Parametric Investigation by Use of a Single-Channel Micromodel. *SPE J.* **2017**, *22* (5), 1362−1373.
(125) Song, W.; Kovscek, A. R. Functionalization of Micromodels with Kaolinite for Investigation of Low Salinity Oil-Recovery Processes. *Lab Chip* **2015**, *15* (16), 3314−3325.
(126) Li, S.; Liu, Y.; Xue, L.; Yang, L.; Yuan, Z. Experimental Investigation on the Pore-Scale Mechanism of Improved Sweep Efficiency by Low-Salinity Water Flooding Using a Reservoir-on-a-Chip. *ACS Omega* **2021**, *6* (32), 20984−20991.
(127) Morishita, R.; Matsuyama, R.; Ishiwata, T.; Tsuchiya, Y.; Giang, P. T.; Takahashi, S. Oil and Water Interactions during Low-Salinity Enhanced Oil Recovery in Water-Wet Porous Media. *Energy Fuels* **2020**, *34* (5), 5258−5266.
(128) Al-Shalabi, E. W.; Sepehrnoori, K. A Comprehensive Review of Low Salinity/Engineered Water Injections and Their Applications in Sandstone and Carbonate Rocks. *J. Pet. Sci. Eng.* **2016**, *139*, 137−161.
(129) Wei, B.; Lu, L.; Li, Q.; Li, H.; Ning, X. Mechanistic Study of Oil/Brine/Solid Interfacial Behaviors during Low-Salinity Waterflooding Using Visual and Quantitative Methods. *Energy Fuels* **2017**, *31* (6), 6615−6624.
(130) Park, S. W.; Lee, J.; Yoon, H.; Shin, S. Microfluidic Investigation of Salinity-Induced Oil Recovery in Porous Media during Chemical Flooding. *Energy Fuels* **2021**, *35* (6), 4885−4892.
(131) Pogaku, R.; Fuat, N. H. M.; Sakar, S.; Cha, Z. W.; Musa, N.; Tajudin, D. N. A. A.; Morris, L. O. Polymer Flooding and Its Combinations with Other Chemical Injection Methods in Enhanced Oil Recovery. *Polym. Bull.* **2018**, *75* (4), 1753−1774.
(132) Wegner, J.; Hincapie, R. E.; Födisch, H.; Ganzer, L. Novel Visualisation of Chemical EOR Flooding Using a Lab-on-a-Chip Setup Supported by an Extensive Rheological Characterisation. *Society of Petroleum Engineers - SPE Asia Pacific Enhanced Oil Recovery Conference, EORC 2015*, Kuala Lumpur, Malaysia, August 11−13, 2015; OnePetro, 2015; SPE-174648-MS.
(133) Meybodi, H. E.; Kharrat, R.; Ghazanfari, M. H. Effect of Heterogeneity of Layered Reservoirs on Polymer Flooding: An Experimental Approach Using Five-Spot Glass Micromodel. *70th Eur. Assoc. Geosci. Eng. Conf. Exhib. 2008 Leveraging Technol. Inc. SPE Eur. 2008*, Rome, Italy, June 9−12, 2008; OnePetro, 2008; SPE-113820-MS.
(134) Kawale, D.; Marques, E.; Zitha, P. L. J.; Kreutzer, M. T.; Rossen, W. R.; Boukany, P. E. Elastic Instabilities during the Flow of Hydrolyzed Polyacrylamide Solution in Porous Media: Effect of Pore-Shape and Salt. *Soft Matter* **2017**, *13* (4), 765−775.
(135) Wang, D.; Xia, H.; Liu, Z.; Yang, Q.Study of the Mechanism of Polymer Solution with Visco-Elastic Behavior Increasing Microscopic Oil Displacement Efficiency and the Forming of Steady "Oil Thread" Flow Channels. *SPE Asia Pacific Oil and Gas Conference and Exhibition*, Jakarta, Indonesia, April 17−19, 2001; OnePetro, 2001; SPE-68723-MS.
(136) Dupas, A.; Hénaut, I.; Argillier, J.-F.; Aubry, T. Mechanical Degradation Onset of Polyethylene Oxide Used as a Hydrosoluble Model Polymer for Enhanced Oil Recovery. *Oil Gas Sci. Technol. − Rev. d'IFP Energies Nouv.* **2012**, *67* (6), 931−940.
(137) Yun, W.; Kovscek, A. R. Microvisual Investigation of Polymer Retention on the Homogeneous Pore Network of a Micromodel. *J. Pet. Sci. Eng.* **2015**, *128*, 115−127.
(138) She, Y.; Aoki, H.; Wang, W.; Li, Z.; Nasir, M.; Mahardika, M. A.; Patmonoaji, A.; Matsushita, S.; Suekane, T. Spontaneous Deformation of Oil Clusters Induced by Dual Surfactants for Oil Recovery: Dynamic Study from Hele-Shaw Cell to Wettability-Altered Micromodel. *Energy Fuels* **2022**, *36* (11), 5762−5774.
(139) Yang, W.; Lu, J.; Wei, B.; Yu, H.; Liang, T. Micromodel Studies of Surfactant Flooding for Enhanced Oil Recovery: A Review. *ACS Omega* **2021**, *6* (9), 6064−6069.

https://doi.org/10.1021/acs.energyfuels.2c01943
Energy Fuels 2022, 36, 9904−9931

(140) Yu, F.; Jiang, H.; Xu, F.; Fan, Z.; Su, H.; Li, J. New Insights into Flow Physics in the EOR Process Based on 2.5D Reservoir Micromodels. *J. Pet. Sci. Eng.* **2019**, *181* (May), 106214.
(141) Yu, F.; Jiang, H.; Ma, M.; Xu, F.; Su, H.; Jia, J. Visualization the Surfactant Imbibition at Pore Scale by Using of Fractured Micromodels. *SPE Improved Oil Recovery Conference*, Virtual, August 31−September 4, 2020; OnePetro, 2020; SPE-200349-MS.
(142) Zhao, X.; Feng, Y.; Liao, G.; Liu, W. Visualizing In-Situ Emulsification in Porous Media during Surfactant Flooding: A Microfluidic Study. *J. Colloid Interface Sci.* **2020**, *578*, 629−640.
(143) Mohammadi, S.; Hossein Ghazanfari, M.; Masihi, M. A Pore-Level Screening Study on Miscible/Immiscible Displacements in Heterogeneous Models. *J. Pet. Sci. Eng.* **2013**, *110*, 40−54.
(144) Yang, W.; Fu, C.; Du, Y.; Xu, K.; Balhoff, M. T.; Weston, J.; Lu, J. Dynamic Contact Angle Reformulates Pore-Scale Fluid-Fluid Displacement at Ultralow Interfacial Tension. *SPE J.* **2021**, *26* (3), 1278−1289.
(145) Dong, M.; Liu, Q.; Li, A. Micromodel Study of the Displacement Mechanisms of Enhanced Heavy Oil Recovery. *International Symposium of the Society of Core Analysts*, Calgary, AB, Canada, September 10−12,2007; SCA2007-47.
(146) Pei, H.; Zhang, G.; Ge, J.; Jin, L.; Ma, C. Potential of Alkaline Flooding to Enhance Heavy Oil Recovery through Water-in-Oil Emulsification. *Fuel* **2013**, *104*, 284−293.
(147) Alzahid, Y.; Mostaghimi, P.; Warkiani, M. E.; Armstrong, R. T.; Joekar-Niasar, V.; Karadimitriou, N.Alkaline Surfactant Polymer Flooding: What Happens at the Pore Scale?. *SPE Europec featured at 79th EAGE Conference and Exhibition*, Paris, France, June 12−15, 2017; OnePetro, 2017; SPE-185832-MS.
(148) Nie, D.; Li, Y.; Li, X.; Zhou, X.; Zhang, F. Evaluation of the Factors Influencing Residual Oil Evolution after Alkali/Surfactant/Polymer Flooding in Daqing Oilfield. *Energies* **2022**, *15*, 3927.
(149) Sedaghat, M.; Mohammadzadeh, O.; Kord, S.; Chatzis, I. Heavy Oil Recovery Using ASP Flooding: A Pore-Level Experimental Study in Fractured Five-Spot Micromodels. *Can. J. Chem. Eng.* **2016**, *94* (4), 779−791.
(150) El-Diasty, A. I.; Aly, A. M. Understanding the Mechanism of Nanoparticles Applications in Enhanced Oil Recovery. *SPE North Africa Technical Conference and Exhibition*, Cairo, Egypt, September 14−16, 2015; OnePetro, 2015; SPE-175806-MS.
(151) Rostami, P.; Sharifi, M.; Aminshahidy, B.; Fahimpour, J. The Effect of Nanoparticles on Wettability Alteration for Enhanced Oil Recovery: Micromodel Experimental Studies and CFD Simulation. *Pet. Sci.* **2019**, *16* (4), 859−873.
(152) Li, R.; Jiang, P.; Gao, C.; Huang, F.; Xu, R.; Chen, X. Experimental Investigation of Silica-Based Nanofluid Enhanced Oil Recovery: The Effect of Wettability Alteration. *Energy Fuels* **2017**, *31* (1), 188−197.
(153) Hendraningrat, L.; Shidong, L.; Torsæter, S.; Torsæter, O. A Glass Micromodel Experimental Study of Hydrophilic Nanoparticles Retention for EOR Project. *SPE Russian Oil and Gas Exploration and Production Technical Conference and Exhibition*, Moscow, Russia, October 16−18, 2012; OnePetro, 2012; SPE-159161-MS.
(154) Cheraghian, G. Effects of Titanium Dioxide Nanoparticles on the Efficiency of Surfactant Flooding of Heavy Oil in a Glass Micromodel. *Pet. Sci. Technol.* **2016**, *34* (3), 260−267.
(155) Khezrnejad, A.; James, L. A.; Johansen, T. E. Water Enhancement Using Nanoparticles in Water Alternating Gas (WAG) Micromodel Experiments. *SPE Annual Technical Conference and Exhibition*, Amsterdam, The Netherlands, October 27−29, 2014; OnePetro, 2014; SPE-173484-STU.
(156) Seright, R. S.; Lang, J. Survey of Field Applications of Gel Treatments for Water Shutoff. *SPE Latin America/Caribbean Petroleum Engineering Conference*, Buenos Aires, Argentina, April 27−29, 1994; OnePetro, 1994; SPE-26991-MS
(157) Hasankhani, G. M.; Madani, M.; Esmaeilzadeh, F.; Mowla, D. Experimental Investigation of Asphaltene-Augmented Gel Polymer Performance for Water Shut-off and Enhancing Oil Recovery in Fractured Oil Reservoirs. *J. Mol. Liq.* **2019**, *275*, 654−666.
(158) Al-Sharji, H. H.; Grattoni, C. A.; Dawe, R. A.; Zimmerman, R. W. Flow of Oil and Water Through Elastic Polymer Gels. *Oil Gas Sci. Technol.* **2001**, *56* (2), 145−152.
(159) Al-Sharji, H. H. Experimental Observation and Measurement of the Flow of Water and Oil through Polymer Gels. 2000.
(160) Liang, B.; Jiang, H.; Li, J.; Seright, R. S.; Lake, L. W. Further Insights into the Mechanism of Disproportionate Permeability Reduction. *SPE Annual Technical Conference and Exhibition*, San Antonio, TX, October 9−11, 2017; OnePetro, 2017; SPE-187364-MS.
(161) Bai, B.; Li, L.; Liu, Y.; Liu, H.; Wang, Z.; You, C. Preformed Particle Gel for Conformance Control. *SPE Reserv. Eval. Eng.* **2007**, *10* (4), 415−422.
(162) Bai, B.; Liu, Y.; Coste, J. P.; Li, L. Preformed Particle Gel for Conformance Control: Transport Mechanism through Porous Media. *Proc. - SPE Symp. Improv. Oil Recover.* **2004**, *2004-April* (January 2004), 17−21.
(163) Zhang, H.; Bai, B. Preformed-Particle-Gel Transport through Open Fractures and Its Effect on Water Flow. *SPE J.* **2011**, *16* (2), 388−400.
(164) Aqcheli, F.; Baghban Salehi, M.; Taghikhani, V.; Pahlevani, H. Synthesis of a Custom-Made Suspension of Preformed Particle Gel with Improved Strength Properties and Its Application in the Enhancement of Oil Recovery in a Micromodel Scale. *J. Pet. Sci. Eng.* **2021**, *207* (June), 109108.
(165) Heidari, S.; Ahmadi, M.; Esmaeilzadeh, F.; Mowla, D. Oil Recovery from Fractured Reservoirs Using in Situ and Preformed Particle Gels in Micromodel Structures. *J. Pet. Explor. Prod. Technol.* **2019**, *9* (3), 2309−2317.
(166) Louf, J. F.; Lu, N. B.; O'Connell, M. G.; Cho, H. J.; Datta, S. S. Under Pressure: Hydrogel Swelling in a Granular Medium. *Sci. Adv.* **2021**, *7* (7), 1−11.
(167) Liu, J.; Almakimi, A.; Wei, M.; Bai, B.; Hussein, I. A. A Comprehensive Review of Experimental Evaluation Methods and Results of Polymer Micro/Nanogels for Enhanced Oil Recovery and Reduced Water Production. *Fuel* **2022**, *324*, 124664.
(168) Wang, S.; Tang, Z.; Qu, J.; Wu, T.; Liu, Y.; Wang, J.; Liu, X.; Ju, Y.; Liu, F. Research on the Mechanisms of Polyacrylamide Nanospheres with Different Size Distributions in Enhanced Oil Recovery. *RSC Adv.* **2021**, *11* (10), 5763−5772.
(169) Hua, Z.; Lin, M.; Dong, Z.; Li, M.; Zhang, G.; Yang, J. Study of Deep Profile Control and Oil Displacement Technologies with Nanoscale Polymer Microspheres. *J. Colloid Interface Sci.* **2014**, *424*, 67−74.
(170) Wyss, H. M.; Franke, T.; Mele, E.; Weitz, D. A. Capillary Micromechanics: Measuring the Elasticity of Microscopic Soft Objects. *Soft Matter* **2010**, *6* (18), 4550−4555.
(171) Yao, C.; Liu, B.; Li, L.; Zhang, K.; Lei, G.; Steenhuis, T. S. Transport and Retention Behaviors of Deformable Polyacrylamide Microspheres in Convergent-Divergent Microchannels. *Environ. Sci. Technol.* **2020**, *54* (17), 10876−10884.
(172) Li, S.; Yu, H.; Li, T.; De; Chen, Z.; Deng, W.; Anbari, A.; Fan, J. Understanding Transport of an Elastic, Spherical Particle through a Confining Channel. *Appl. Phys. Lett.* **2020**, *116* (10), 103705.
(173) Li, S.; Yu, H. H.; Fan, J. Modeling Transport of Soft Particles in Porous Media. *Phys. Rev. E* **2021**, *104* (2), 1−9.
(174) Yao, C.; Lei, G.; Hou, J.; Xu, X.; Wang, D.; Steenhuis, T. S. Enhanced Oil Recovery Using Micron-Size Polyacrylamide Elastic Microspheres: Underlying Mechanisms and Displacement Experiments. *Ind. Eng. Chem. Res.* **2015**, *54* (43), 10925−10934.
(175) Zhang, L.; Abbaspourrad, A.; Parsa, S.; Tang, J.; Cassiola, F.; Zhang, M.; Tian, S.; Dai, C.; Xiao, L.; Weitz, D. A. Core-Shell Nanohydrogels with Programmable Swelling for Conformance Control in Porous Media. *ACS Appl. Mater. Interfaces* **2020**, *12* (30), 34217−34225.
(176) Zhang, Y.; Geng, J.; Liu, J.; Bai, B.; He, X.; Wei, M.; Deng, W. Direct Pore-Level Visualization and Verification of in Situ Oil-in-Water Pickering Emulsification during Polymeric Nanogel Flooding

https://doi.org/10.1021/acs.energyfuels.2c01943
Energy Fuels 2022, 36, 9904−9931

for EOR in a Transparent Three-Dimensional Micromodel. *Langmuir* **2021**, *37* (45), 13353−13364.
(177) Kovscek, A. R.; Radke, C. J. *Fundamentals of Foam Transport in Porous Media*; Lawrence Berkeley Lab.: Berkeley, CA, 1993.
(178) Yu, W.; Kanj, M. Y. Review of Foam Stability in Porous Media: The Effect of Coarsening. *J. Pet. Sci. Eng.* **2022**, *208* (PD), 109698.
(179) Jiménez, A. I.; Radke, C. J. *Dynamic Stability of Foam Lamellae Flowing through a Periodically Constricted Pore*; ACS Publications, 1989.
(180) Jones, S. A.; Getrouw, N.; Vincent-Bonnieu, S. Foam Flow in a Model Porous Medium: I. the Effect of Foam Coarsening. *Soft Matter* **2018**, *14* (18), 3490−3496.
(181) Gauteplass, J.; Chaudhary, K.; Kovscek, A. R.; Fernø, M. A. Pore-Level Foam Generation and Flow for Mobility Control in Fractured Systems. *Colloids Surfaces A Physicochem. Eng. Asp.* **2015**, *468*, 184−192.
(182) Lu, T.; Li, Z.; Hou, D.; Xu, Z.; Ban, X.; Zhou, B. Experimental and Numerical Evaluation of Surfactant-Nanoparticles Foam for Enhanced Oil Recovery under High Temperature. *Energy Fuels* **2020**, *34* (1), 1005−1013.
(183) Bai, Y.; Shang, X.; Wang, Z.; Zhao, X.; Dong, C. Experimental Investigation of Nanolaponite Stabilized Nitrogen Foam for Enhanced Oil Recovery. *Energy Fuels* **2018**, *32* (3), 3163−3175.
(184) Zhou, W.; Xin, C.; Chen, S.; Yu, Q.; Wang, K. Polymer-Enhanced Foam Flooding for Improving Heavy Oil Recovery in Thin Reservoirs. *Energy Fuels* **2020**, *34* (4), 4116−4128.
(185) Wang, F.; Chen, H.; Alzobaidi, S.; Li, Z. Application and Mechanisms of Self-Generated Heat Foam for Enhanced Oil Recovery. *Energy Fuels* **2018**, *32* (9), 9093−9105.
(186) Zhang, H.; Chen, G.; Dong, M.; Zhao, S.; Liang, Z. Evaluation of Different Factors on Enhanced Oil Recovery of Heavy Oil Using Different Alkali Solutions. *Energy and Fuels.* **2016**, *30*, 3860−3869.
(187) Mahardika, M. A.; She, Y.; Shori, F.; Patmonoaji, A.; Matsushita, S.; Suekane, T.; Nagatsu, Y. Enhanced Heavy Oil Recovery by Calcium Hydroxide Flooding with the Production of Viscoelastic Materials: Study with 3-D X-Ray Tomography and 2-D Glass Micromodels. *Energy Fuels* **2021**, *35* (14), 11210−11222.
(188) Nagatsu, Y.; Abe, K.; Konmoto, K.; Omori, K. Chemical Flooding for Enhanced Heavy Oil Recovery via Chemical-Reaction-Producing Viscoelastic Material. *Energy Fuels* **2020**, *34* (9), 10655−10665.
(189) Mohammadzadeh, O.; Chatzis, I. Analysis of the Heat Losses Associated with the SAGD Visualization Experiments. *J. Pet. Explor. Prod. Technol.* **2016**, *6* (3), 387−400.
(190) De Haas, T. W.; Fadaei, H.; Guerrero, U.; Sinton, D. Steam-on-a-Chip for Oil Recovery: The Role of Alkaline Additives in Steam Assisted Gravity Drainage. *Lab Chip* **2013**, *13* (19), 3832−3839.
(191) Zhao, H.; Pierobon, S.; Pettigrew, A.; Doan-Prevost, J.; Garnier, O. F.; De Haas, T. Measurement of Propane and Butane Diffusion into Heavy Oil Using Microfluidics - Is Small Better? *Abu Dhabi International Petroleum Exhibition & Conference*, Abu Dhabi, UAE, November 12−15, 2019; OnePetro, 2019; SPE-193015-MS.
(192) Karadimitriou, N. K.; Nuske, P.; Kleingeld, P. J.; Hassanizadeh, S. M.; Helmig, R. Simultaneous Thermal and Optical Imaging of Two-Phase Flow in a Micro-Model. *Lab Chip* **2014**, *14* (14), 2515−2524.
(193) Qi, Z. B.; Abedini, A.; Lele, P.; Mosavat, N.; Guerrero, A.; Sinton, D. Pore-Scale Analysis of Condensing Solvent Bitumen Extraction. *Fuel* **2017**, *193*, 284−293.
(194) Wood, D. A. Microbial Improved and Enhanced Oil Recovery (Mieor): Review of a Set of Technologies Diversifying Their Applications. *Adv. Geo-Energy Res.* **2019**, *3* (2), 122−140.
(195) Kryachko, Y. Novel Approaches to Microbial Enhancement of Oil Recovery. *J. Biotechnol.* **2018**, *266* (July 2017), 118−123.
(196) Armstrong, R. T.; Wildenschild, D. Investigating the Pore-Scale Mechanisms of Microbial Enhanced Oil Recovery. *J. Pet. Sci. Eng.* **2012**, *94*−*95*, 155−164.
(197) Abolhasanzadeh, A.; Khaz'Ali, A. R.; Hashemi, R.; Jazini, M. Experimental Study of Microbial Enhanced Oil Recovery in Oil-Wet Fractured Porous Media. *Oil Gas Sci. Technol.* **2020**, *75*, 73.
(198) Khajepour, H.; Mahmoodi, M.; Biria, D.; Ayatollahi, S. Investigation of Wettability Alteration through Relative Permeability Measurement during MEOR Process: A Micromodel Study. *J. Pet. Sci. Eng.* **2014**, *120*, 10−17.
(199) Gaol, C. L.; Ganzer, L.; Mukherjee, S.; Alkan, H. Parameters Govern Microbial Enhanced Oil Recovery (MEOR) Performance in Real-Structure Micromodels. *J. Pet. Sci. Eng.* **2021**, *205* (March), 108814.
(200) Wang, X.; Zhu, W.; Li, H.; Song, Z. Pore-Scale Mechanisms of the Synergistic Effects between Microbial Cultures and Chemical Surfactants on Oil Recovery. *Energy Fuels* **2018**, *32* (12), 12319−12327.
(201) Zou, C.; Yang, Z.; Zhu, R.; Zhang, G.; Hou, L.; Wu, S.; Tao, S.; Yuan, X.; Dong, D.; Wang, Y.; Wang, L.; Huang, J.; Wang, S. Progress in China's Unconventional Oil & Gas Exploration and Development and Theoretical Technologies. *Acta Geologica Sinica* **2015**, *89* (3), 938−971.
(202) Phan, V. N.; Nguyen, N. T.; Yang, C.; Joseph, P.; Gué, A. M. Fabrication and Experimental Characterization of Nanochannels. *J. Heat Transfer* **2012**, *134* (5), 1−6.
(203) Tas, N. R.; Mela, P.; Kramer, T.; Berenschot, J. W.; Van Den Berg, A. Capillarity Induced Negative Pressure of Water Plugs in Nanochannels. *Nano Lett.* **2003**, *3* (11), 1537−1540.
(204) Bao, B.; Zandavi, S. H.; Li, H.; Zhong, J.; Jatukaran, A.; Mostowfi, F.; Sinton, D. Bubble Nucleation and Growth in Nanochannels. *Phys. Chem. Chem. Phys.* **2017**, *19* (12), 8223−8229.
(205) Zhong, J.; Zhao, Y.; Lu, C.; Xu, Y.; Jin, Z.; Mostowfi, F.; Sinton, D. Nanoscale Phase Measurement for the Shale Challenge: Multicomponent Fluids in Multiscale Volumes. *Langmuir* **2018**, *34* (34), 9927−9935.
(206) Jatukaran, A.; Zhong, J.; Persad, A. H.; Xu, Y.; Mostowfi, F.; Sinton, D. Direct Visualization of Evaporation in a Two-Dimensional Nanoporous Model for Unconventional Natural Gas. *ACS Appl. Nano Mater.* **2018**, *1* (3), 1332−1338.
(207) Ally, J.; Molla, S.; Mostowfi, F. Condensation in Nanoporous Packed Beds. *Langmuir* **2016**, *32* (18), 4494−4499.
(208) Yang, Q.; Jin, B.; Banerjee, D.; Nasrabadi, H. Direct Visualization and Molecular Simulation of Dewpoint Pressure of a Confined Fluid in Sub-10 Nm Slit Pores. *Fuel* **2019**, *235* (September 2018), 1216−1223.
(209) Wu, Q.; Ok, J. T.; Sun, Y.; Retterer, S. T.; Neeves, K. B.; Yin, X.; Bai, B.; Ma, Y. Optic Imaging of Single and Two-Phase Pressure-Driven Flows in Nano-Scale Channels. *Lab Chip* **2013**, *13* (6), 1165−1171.
(210) Wu, Q.; Bai, B.; Ma, Y.; Ok, J. T.; Neeves, K. B.; Yin, X. Optic Imaging of Two-Phase-Flow Behavior in 1D Nanoscale Channels. *SPE J.* **2014**, *19* (5), 793−802.
(211) Liu, S.; Wu, Q.; Bai, B.; Ma, Y.; Wei, M.; Yin, X.; Neeves, K. Optic Imaging of Oil/Water Flow Behavior in Nano-Scale Channels. *SPE Improved Oil Recovery Symposium*, Tulsa, OK, April 12−16, 2014; OnePetro, 2014; SPE-169111-MS.
(212) Zhong, J.; Abedini, A.; Xu, L.; Xu, Y.; Qi, Z.; Mostowfi, F.; Sinton, D. Nanomodel Visualization of Fluid Injections in Tight Formations. *Nanoscale* **2018**, *10* (46), 21994−22002.
(213) Kelly, S. Experimental Investigation of the Influence of Molecular Surface Interactions on Imbibition in Shale Nano-Pore Proxies. *Proc. - SPE Annu. Technol. Conf. Exhib.* **2013**, *7*, 5570−5581.
(214) Sinton, D. Energy: The Microfluidic Frontier. *Lab on a Chip.* **2014**, *14*, 3127−3134.
(215) Hasham, A. A.; Abedini, A.; Jatukaran, A.; Persad, A.; Sinton, D. Visualization of Fracturing Fluid Dynamics in a Nanofluidic Chip. *J. Pet. Sci. Eng.* **2018**, *165* (November2017), 181−186.
(216) Mehmani, A.; Kelly, S.; Torres-Verdin, C.; Balhoff, M. Quantification of Fracture-Matrix Fluid Transport in Unconventional Rocks Using Two-Scale Microfluidic Chips. *SPE/AAPG/SEG*

https://doi.org/10.1021/acs.energyfuels.2c01943
Energy Fuels 2022, 36, 9904−9931

Unconventional Resources Technology Conference, Austin, TX, July 24–26, 2017; OnePetro, 2017; URTEC-2669314-MS.
(217) Fattahi Mehraban, M.; Farzaneh, S. A.; Sohrabi, M.; Sisson, A. Novel Insights into the Pore-Scale Mechanism of Low Salinity Water Injection and the Improvements on Oil Recovery. *Energy Fuels* **2020**, *34* (10), 12050–12064.
(218) Kiani, S.; Rogers, S. E.; Sagisaka, M.; Alexander, S.; Barron, A. R. A New Class of Low Surface Energy Anionic Surfactant for Enhanced Oil Recovery. *Energy Fuels* **2019**, *33* (4), 3162–3175.
(219) Sedaghat, M.; Mohammadzadeh, O.; Kord, S.; Chatzis, I. Pore-Level Experimental Investigation of ASP Flooding to Recover Heavy Oil in Fractured Five-Spot Micromodels. *EUROPEC 2015*, Madrid, Spain, June 1–4, 2015; OnePetro, 2015; SPE-174290-MS.
(220) Wang, D.; Sun, S.; Sha, T.; Liu, T.; Dong, H.; Cui, K.; Li, H.; Gong, Y.; Hou, J.; Zhang, Z.; Fu, P. Synergistic Effect of Silica Nanoparticles and Rhamnolipid on Wettability Alteration of Low Permeability Sandstone Rocks. *Energy Fuels* **2018**, *32* (8), 8098–8107.
(221) Liu, Y.; Zou, C.; Zhou, D.; Li, H.; Gao, M.; Zhao, G.; Dai, C. Novel Chemical Flooding System Based on Dispersed Particle Gel Coupling In-Depth Profile Control and High Efficient Oil Displacement. *Energy Fuels* **2019**, *33* (4), 3123–3132.
(222) Tao, J.; Dai, C.; Kang, W.; Zhao, G.; Liu, Y.; Fang, J.; Gao, M.; You, Q. Experimental Study on Low Interfacial Tension Foam for Enhanced Oil Recovery in High-Temperature and High-Salinity Reservoirs. *Energy Fuels* **2017**, *31* (12), 13416–13426.
(223) Chen, H.; Li, Z.; Wang, F.; Li, S. Investigation on in Situ Foam Technology for Enhanced Oil Recovery in Offshore Oilfield. *Energy Fuels* **2019**, *33* (12), 12308–12318.
(224) Zhong, J.; Zandavi, S. H.; Li, H.; Bao, B.; Persad, A. H.; Mostowfi, F.; Sinton, D. Condensation in One-Dimensional Dead-End Nanochannels. *ACS Nano* **2017**, *11* (1), 304–313.
(225) Kong, L.; Ishutov, S.; Hasiuk, F.; Xu, C. 3D Printing for Experiments in Petrophysics, Rock Physics, and Rock Mechanics: A Review. *SPE Reserv. Eval. Eng.* **2021**, *24* (4), 721–732.
(226) Zhao, Y.; Jiang, H.; Li, J.; Wang, C.; Gao, Y.; Yu, F.; Su, H. Study on the Classification and Formation Mechanism of Microscopic Remaining Oil in High Water Cut Stage Based on Machine Learning. *Abu Dhabi International Petroleum Exhibition & Conference*, Abu Dhabi, UAE, November 13–16, 2017; OnePetro, 2017; SPE-188228-MS.
(227) Blunt, M. J.; Bijeljic, B.; Dong, H.; Gharbi, O.; Iglauer, S.; Mostaghimi, P.; Paluszny, A.; Pentland, C. Pore-Scale Imaging and Modelling. *Adv. Water Resour.* **2013**, *51*, 197–216.
(228) Tseng, P.; Weaver, W. M.; Masaeli, M.; Owsley, K.; Di Carlo, D. Research Highlights: Microfluidics Meets Big Data. *Lab Chip* **2014**, *14* (5), 828–832.
(229) Riordon, J.; Sovilj, D.; Sanner, S.; Sinton, D.; Young, E. W. K. Deep Learning with Microfluidics for Biotechnology. *Trends Biotechnol.* **2019**, *37* (3), 310–324.
(230) Momtahen, S.; Al-Obaidy, F.; Mohammadi, F. Machine Learning with Digital Microfluidics for Drug Discovery and Development. *2019 IEEE Canadian Conference of Electrical and Computer Engineering (CCECE)*, Edmonton, AB, Canada, May 5–8, 2019; IEEE: New York, 2019; pp 8–13.
(231) Ibrahim, M.; Chakrabarty, K.; Zeng, J. BioCyBig: A Cyberphysical System for Integrative Microfluidics-Driven Analysis of Genomic Association Studies. *IEEE Trans. Big Data* **2020**, *6* (4), 609–623.
(232) Galan, E. A.; Zhao, H.; Wang, X.; Dai, Q.; Huck, W. T. S.; Ma, S. Intelligent Microfluidics: The Convergence of Machine Learning and Microfluidics in Materials Science and Biomedicine. *Matter* **2020**, *3* (6), 1893–1922.

https://doi.org/10.1021/acs.energyfuels.2c01943
Energy Fuels 2022, 36, 9904–9931